Spin Polarization versus Spin Delocalization. Topological Electron and Spin Density Analysis of the Rotational Automerization of Allyl Radical Including Electron Correlation Effects[1]

Rainer Glaser* and Godwin Sik-Cheung Choy

Department of Chemistry, University of Missouri−Columbia, Columbia, Missouri 65211

Received: May 30, 1994; In Final Form: August 11, 1994[⊗]

The rotational automerization **A** ⇌ **B**‡ ⇌ **A** of allyl radical was examined at the levels UHF, PUHF, MP2, CID, CCD, CISD, and QCISD. Analyses of the reaction path, of vibrational modes, and of activation energies show methodological deficiencies at the MP2, CID, CCD, and CISD levels which are not related in a simple fashion to the spin contamination of the reference wave functions. Graphical analysis of electron and spin density functions and electron and spin populations reveal the underlying fundamental problem. The *electron density relaxation* always is described well along the automerization path, but the *spin density relaxations* differ greatly. All post-HF methods affect the spin density qualitatively in the same way: Correlation increases the importance of the interaction of the unpaired spin with the spins of the paired electrons via the *spin delocalization mechanism* relative to the *spin polarization mechanism*. However, the methods differ greatly in the relative importance of these mechanisms, and significantly different spin density distributions within the ethene part of **B** are the consequence. QCISD theory yields results that are in very good agreement with all available experimental data. The results corroborate that the PUHF method represents a valuable alternative for studies of spin density distributions in general and the method of choice for large radicals.

Introduction

Allyl radical is an important intermediate in hydrocarbon combustion and pyrolysis,[3] photochemical reactions,[4] and surface catalysis.[5] Allyl radical has been well characterized by various spectroscopic methods including electron diffraction,[6] electron spin resonance[7] (ESR), photoelectron spectroscopy[8] (PE), infrared resonance spectroscopy[9] (IR), and Raman spectroscopy.[10] Experimentally, C_{2v} symmetry was established for the ground state of allyl radical. The correct theoretical reproduction of the symmetry of allyl radical −delocalized radical **I** with C_{2v} symmetry versus localized radical **II** with C_s symmetry−led to important advances in the understanding of instability problems in Hartree−Fock theory. McKelvey and

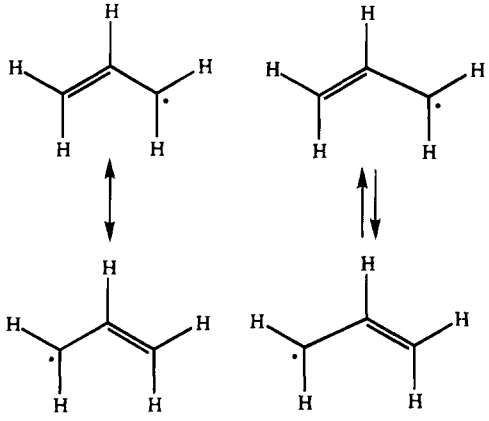

I, C_{2v} **II, C_s**

Hehre[11] studied the symmetry dilemma of allyl radical at the RHF/STO-3G level and concluded that the energy difference between the C_{2v} and the C_s structures was due to basis set limitations. McKelvey and Berthier[12] reported that the doublet instability of allyl radical would disappear at the RHF limit. Paldus et al.[13] examined the problem using extended basis sets and concluded that the doublet instability of allyl radical is a common phenomenon at the RHF level. Kikuchi[14] thought that the consideration of single excitations with a RHF reference wave function was sufficient to correct the doublet instability problem, but symmetry breaking still occurred at the CASSCF level using the RHF wave function as reference.[15] While RHF theory failed in predicting the correct geometry of allyl radical, the unrestricted Hartree−Fock method (UHF) was successful in reproducing the C_{2v} symmetric minimum,[16] and this finding remains one of the great successes of UHF theory.

Allyl radical is the simplest radical requiring two degenerate resonance forms for its description, and it is thus an ideal system for studies of resonance[17] and delocalization energies. The allyl resonance energy can be measured experimentally in two ways,[18a] namely, via the determination of the rotational barrier[18b] or via the differences in the dissociation energies of the primary C−H bonds in propane and propene.[18c] The barrier to rotation of 1-deuterated allyl radical was determined to be 15.7 ± 1.0 kcal/mol using ESR spectroscopy.[18b] The free energy of activation to internal rotation at 280 °C is larger than $\Delta G^{\ddagger} >$ 17 kcal/mol.[19] Hammons et al.[20] calculated the rotational barrier at the UHF/6-31G* level to be 18.6 kcal/mol. With the optimized UHF structure and including electron correlation effects, barriers of 12.6, 18.3, and 15.3 kcal/mol, respectively, were found at the levels UMP2, PUMP2, and CISD. Feller et al. examined the rotational barrier at the MCSCF/3-21G level and reported a barrier of 14.1 kcal/mol.[21]

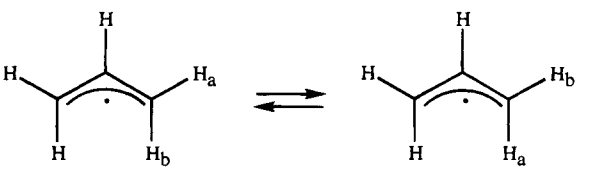

[⊗] Abstract published in *Advance ACS Abstracts*, September 15, 1994.

0022-3654/94/2098-11379$04.50/0

TABLE 1: Total, Relative, and Vibrational Zero-Point Energies

	structure **A**			structure **B**			structure **C**		
method	E_{total}	VZPE[a]		E_{total}[a] (E_{rel})	VZPE		E_{total} (E_{rel})	VZPE	
UHF	−116.468 100	43.62	M	−116.438 510 (18.57)	42.71	TS			
PUHF	−116.485 861			−116.445 497 (25.33)					
MP2	−116.824 292	42.64	M	−116.805 058 (12.07)	44.28	M	−116.804 057 (12.70)	42.80	TS
CID	−116.822 523	42.86	M	−116.799 738 (14.30)	43.77	M	−116.799 603 (14.38)	43.07	TS
CID(sc)[c]	−116.864 108			−116.843 977 (12.63)			−116.843 534 (12.91)		
CCD	−116.861 128	42.18	M	−116.840 525 (12.93)	43.51	M	−116.840 044 (13.23)	42.35	TS
CISD	−116.814 449	42.71	M	−116.790 356 (15.12)	43.17	M	−116.790 351 (15.12)	42.93	TS
CISD(sc)[c]	−116.857 591			−116.834 074 (14.76)			−116.834 090 (14.75)		
QCISD	−116.872 012	41.77	M	−116.847 520 (15.37)	41.05	TS			

[a] Vibrational zero-point energies (VZPE) in kilocalories per mole. M indicates a minimum and TS denotes a transition state structure. [b] Total energies in atomic units. Values in parentheses are the relative energies in kcal/mol with regard to the most stable stationary structure. [c] CISD(sc) and CID(sc) energies are size-consistency-corrected levels.

In this article, we report the results of a study of electron and spin density relaxation effects along the pathway for automerization of allyl radical at higher levels of ab initio theory that include electron correlation effects in various ways. Since previous theoretical studies employed structures that were not optimized at correlated levels, we begin with a reexamination of the potential energy surface of allyl radical including correlated effects in the structure optimizations and we also report vibrational analyses at all of the correlated levels. The analysis of the electron and spin density distributions is in the focus of our study, and results are reported that were determined using unrestricted Hartree−Fock theory without (UHF) and with (PUHF) annihilation of spin contaminants as well as using various post-Hartree−Fock methods. Effects of dynamic electron correlation on the rotational barrier of allyl radical were studied with second-order Møller−Plesset perturbation theory (MP2), configuration interaction theory with double excitation (CID) and with single and double excitations (CISD), coupled cluster theory with double excitation (CCD), and quadratic CI theory with single and double excitations (QCISD). While UHF, PUHF, and QCISD theory provide good to excellent results, severe methodological deficiencies were discovered at all of the other levels. The performances of the methods are analyzed in detail, and compelling evidence is provided demonstrating in a rigorous fashion that these artifacts all are related to method-dependent differences in the estimation of the relative importance of the interactions of the unpaired electron spin with the paired electrons via the spin polarization and spin delocalization mechanisms in the transition state conformation of allyl radical.

Computational Methods

Geometry optimizations were performed within the symmetry point groups specified with Schlegel's gradient algorithm implemented in Gaussian92.[22] The exact Hessian matrix for each structure was computed at all theoretical levels to determine harmonic vibrational frequencies and vibrational zero-point energies (VZPEs) and to establish the character of the stationary structures (minimum or transition state) via the number of negative eigenvalues. The higher theoretical levels considered include MP2, CID, CCD, CISD, and QCISD theory. The basis set 6-31G*[23] was used throughout, and the UHF wave function always served as the reference. Core electrons were included in all calculations of electron correlation energies except at the CISD level. Highly reliable activation energies also can be obtained using higher order Møller−Plesset perturbation theory. Full fourth-order Møller−Plesset perturbation calculations were carried out within the frozen core approximation and with the fully polarized valence triple-ζ basis set 6-311G** based on the MP2(full)/6-31G* optimized structures.

Electron and spin density analyses were carried out at the UHF level without and with annihilation of contaminations due to the next higher spin state (PUHF) and at the correlated levels MP2, CID, CCD, CISD, and QCISD. The correlated densities were calculated with the Z vector method.[24] Nonstandard routes were used to write the density matrices to the Gaussian output files, and the density matrices were then transformed into a format suitable as input to the electron and spin density analysis programs using the programs DENCUT, DENADD, and PSIPUHF.[2] Topological and integrated properties of the electron density functions were determined with the programs SADDLE_PUHF and PROAIM_PUHF.[25] Cross sections of the electron and spin densities were determined with the program NETZ.[26]

Results and Discussion

Potential Energy Surface Analysis. Table 1 lists total and relative energies and vibrational zero-point energies together with the characters of the stationary structures for all theoretical levels. Relative energies are reported with respect to **A**, and they do not include vibrational zero-point energies. In Table 2, we report the energies obtained at the higher order MPx levels without and after annihilation of spin contaminants via projection. Complete structural data sets are summarized in Table 3.

The three conformations **A** (C_{2v}), **B** (C_s), and **C** (C_1) shown in Figure 1 are pertinent to the discussion of the rotational automerization. At the UHF and QCISD levels, and as expected, structures **A** are minima and structures **B** correspond to the transition state structures for rotation. However, different potential energy hypersurface characteristics occur at the levels MP2, CID, CCD, and CISD, where structures **B** are predicted to be shallow local minima and where the isomerization between the minima **A** and **B** would involve the transition state structures **C**.

We will first discuss the potential energy surfaces and the activation energies predicted at the different levels of theory.

TABLE 2: Total Energies of Allyl Radical at MP4/6-31G//MP2(full)/6-31G*[a]**

method	A	B	C		Δ^b
S^2(UHF)[c]	0.9525	0.7851	0.8345		
MP2	−116.893 792	−116.875 279	−116.874 348	(12.20)	0.58
MP3	−116.928 003	−116.908 248	−116.907 803	(12.68)	0.28
MP4(D)	−116.938 142	−116.919 024	−116.918 429	(12.37)	0.37
MP4(DQ)	−116.930 202	−116.910 165	−116.909 820	(12.79)	0.22
MP4(SDQ)	−116.934 987	−116.913 703	−116.913 744	(13.33)	−0.03
MP4(SDTQ)	−116.948 843	−116.928 644	−116.928 349	(12.86)	0.19
PMP2	−116.907 945	−116.878 848	−116.880 600	(17.16)	−1.10
PMP3	−116.938 457	−116.910 764	−116.912 389	(16.36)	−1.02
PMP4	−116.959 298	−116.931 160	−116.932 935	(16.54)	−1.11

[a] Total energies at MP4/6-311G**//MP2(full)/6-31G* in atomic units. Values given in parentheses are relative energies in kilocalories per mole with regard to the respective most stable stationary structure. [b] Relative energies Δ are defined as $\Delta = |E(\mathbf{C}) - E(\mathbf{B})|$ and given in kcal/mol. $\Delta > 0$ indicates that **B** is more stable than **C**. [c] Eigenvalues of the $\langle S^2 \rangle$ operator of the UHF reference. The eigenvalues all are within 0.001 of 0.75 after annihilation of the unwanted spin states (s+1) or (s+1) to (s+3) for **A**−**C**.

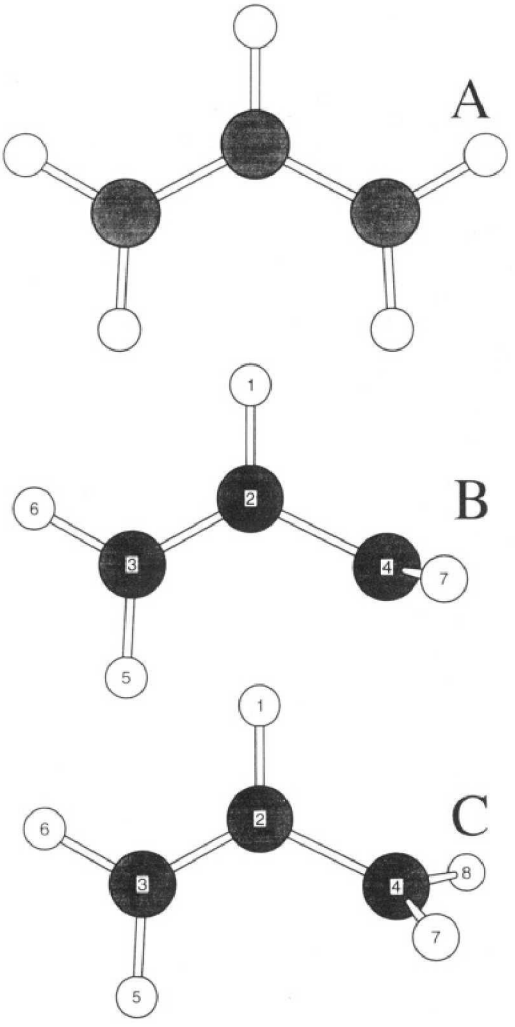

Figure 1. Structures **A** (C_{2v}), **B** (C_s), and **C** (C_1) of allyl radical.

We will then examine methodological differences on structures and examine their relations to the computed activation energies. To convert the activation energies into rotational barriers, vibrational zero-point energy corrections need to be included, and a critical discussion of the computed vibrational properties will thus follow.

Model Dependency of the Rotational Activation Energy. UHF and PUHF. UHF wave functions are spin contaminated due to admixtures of higher spin states.[27] Löwdin showed that the spin contaminations are mainly due to contributions from the next higher spin state. Annihilation of the next higher spin state via spin projection[28,29] (PUHF) corrects efficiently: The $\langle S^2 \rangle$ eigenvalues are 0.973 and 0.836 for **A** and **B**, respectively, at the UHF level, and they are 0.758 (**A**) and 0.752 (**B**) at the PUHF level. Spin projection changes the total energies of **A** and **B** by 11.15 and 4.38 kcal/mol, respectively, and the activation energy is therefore increased very significantly by 6.76 kcal/mol from 18.57 to 25.33 kcal/mol by spin projection.

MP2 and CCD. Energies calculated at the MP2 and CCD levels are not variational, but they are size consistent. Both single and double excitation are considered at the MP2 level, while CCD theory considers only the latter. Pople et al. showed that the CCD energies are of nearly equal quality as the energies obtained with fourth-order Møller−Plesset perturbation theory with double and quartet excitations, MP4(DQ).

Unexpectedly, the **B** structures were found to be *local minima*, and we optimized the transition state structures **C** for isomerization between **A** and **B**. Structures **B** are considerably more stable than structures **C** at MP2 (by 0.63 kcal/mol) and CCD (by 0.30 kcal/mol), and activation energies (**A** versus **C**) of 12.70 and 13.23 kcal/mol, respectively, would result at the levels MP2 and CCD.

We analyzed the relative stabilities of the **B** and **C** structures further with more reliable energy calculations at higher levels of MP theory and with a better basis set,[30] at levels up to MP4-(SDTQ)/6-311G**//MP2(full)/6-31G* (Table 2). These calculations were performed without and with annihilation of the spin contaminants in the UHF reference. Assuming that the spin contamination of the UHF reference causes **B** to occur as a local minimum (or structures **C** to be artificially destabilized),[31] one would expect that the relative energies of **B** and **C** might be reversed at the PMPx levels since spin contaminations are successfully eliminated at these levels, as is evidenced by the $\langle S^2 \rangle$ eigenvalues (Table 3). Yet, the opposite is found. Higher order MP theory reduces ΔE(**B**,**C**), but **B** remains more stable than **C**; at the MP4(SDTQ) level, **B** is preferred over **C** by 0.19 kcal/mol. Thus, we must conclude that MP2 predicts the wrong potential energy hypersurface characteristics for other reasons, and these will be discussed below.

CID, CISD, and QCISD. Unlike MP2 and CCD, the CID and CISD methods are variational but not size-consistent. **B** is more stable than structure **C** by 0.08 kcal/mol at CID, while **B** and **C** have nearly the same energies at CISD. Langhoff and Davidson[32] described a method to correct the energies for size consistency, and, with this Davidson correction considered, **B** is 0.28 kcal/mol more stable than **C** at CID and **C** and **B** are isoenergetic at the CISD level (**C** preference only 1 cal/mol).

The activation energies for rotation at the CID (CISD) levels with and without size-consistency correction are 14.30 (15.12) kcal/mol and 12.63 (14.76) kcal/mol, respectively. Size-consistency corrections reduce the activation energies at both levels. The inclusion of single excitations at the CISD level increases the activation energy by 0.82 and 2.13 kcal/mol, respectively, with and without size-consistency correction.

TABLE 3: Model Dependency on Structures of Allyl Radical

	structures **A**						
parameter	UHF	MP2	CID	CCD	CISD	QCISD	exptl[b]
H1−C2	1.078	1.088	1.085	1.091	1.086	1.091	1.069
C2−C3	1.391	1.377	1.380	1.381	1.383	1.389	1.428
C2−C4							
C3−H5	1.076	1.084	1.082	1.087	1.083	1.088	1.069
C3−H6	1.074	1.082	1.080	1.085	1.081	1.086	1.069
C4−H7							
C4−H8							
∠(H1−C2−C3)	117.74	117.81	117.77	117.77	117.77	117.80	117.7
∠(H1−C2−C4)							
∠(C2−C3−H5)	121.16	120.96	121.10	121.09	121.07	121.04	120.9
∠(C2−C3−H6)	121.42	121.81	121.70	121.77	121.65	121.68	120.9
∠(C2−C4−H7)							
∠(C2−C4−H8)							
∠(C3−C2−C4)	124.52	124.38	124.46	124.46	124.46	124.46	124.40

	structures **B**					
parameter	UHF*	MP2	CID	CCD	CISD	QCISD
H1−C2	1.082	1.092	1.089	1.094	1.090	1.095
C2−C3	1.327	1.305	1.308	1.308	1.313	1.336
C2−C4	1.479	1.475	1.476	1.479	1.477	1.476
C3−C5	1.076	1.085	1.083	1.088	1.083	1.088
C3−H6	1.076	1.085	1.082	1.087	1.083	1.088
C4−H7	1.076	1.082	1.081	1.085	1.082	1.087
C4−H8						
∠(H1−C2−C3)	118.49	118.71	118.73	118.84	118.67	118.48
∠(H1−C2−C4)	116.75	116.32	116.32	116.18	116.41	116.87
∠(C2−C3−H5)	121.78	121.76	121.87	121.92	121.85	121.73
∠C(2−C3−H6)	121.43	121.56	121.55	121.62	121.52	121.48
∠(C3−C4−H7)	120.56	120.23	120.45	120.42	120.49	120.87
∠(C2−C4−H8)						
∠(C3−C2−C4)	124.76	124.97	124.95	124.98	124.92	124.65
ϵ	1.74	2.39	2.41	2.66	2.26	1.61
∠(H1−C2−C3−H5)						
∠(H1−C2−C3−H6)						
∠(H1−C2−C4−H7)	82.82	81.29	82.66	82.56	82.83	84.69
∠(H1−C2−C4−H8)						
∠(C4−C2−H1−C3)						
∠(H7−C4−C2−H8)	165.64	162.58	165.32	165.12	165.66	169.38
δ value		−7.70	−1.96	−4.56	−0.30	

	structures **C**			
parameter	MP2	CID	CCD	CISD
H1−C2	1.092	1.089	1.094	1.090
C2−C3	1.303	1.307	1.307	1.313
C2−C4	1.473	1.476	1.478	1.477
C3−H5	1.085	1.083	1.088	1.083
C3−H6	1.085	1.082	1.087	1.083
C4−H7	1.082	1.081	1.085	1.082
C4−H8	1.082	1.081	1.086	1.082
∠(H1−C2−C3)	118.71	118.72	118.81	118.67
∠(H1−C2−C4)	116.36	116.31	116.22	116.39
∠(C2−C3−H5)	121.82	121.90	121.93	121.87
∠(C2−C3−H6)	121.61	121.58	121.65	121.53
∠(C2−C4−H7)	121.10	120.82	121.02	120.62
∠(C2−C4−H8)	120.38	120.35	120.41	120.41
∠(C3−C2−C4)	124.93	124.97	124.97	124.94
ϵ	2.35	2.41	2.59	2.28
∠(H1−C2−C3−H5)	179.45	179.66	179.60	179.45
∠(H1−C2−C3−H6)	−0.26	−0.17	−0.14	−0.08
∠(H1−C2−C4−H7)	106.96	96.53	102.77	88.55
∠(H1−C2−C4−H8)	−63.32	−70.75	−66.91	−77.41
∠(C4−C2−H1−C3)	180.01	180.03	180.13	180.01
∠(H7−C4−C2−H8)	170.28	167.28	169.68	165.96
δ value				

[a] In angstroms and degrees. [b] Reference 33. The claimed accuracies for the C−C and C−H bonds are ±0.013 and ±0.016 Å, respectively, and ±3.4° for bond angles. The reported C−H bond lengths were the mean values of the C−H bond lengths.

The QCISD method is both size-consistent and variational, and this method is the "best" method among all the theoretical models considered here. The shape of the potential energy hypersurface at this level is the same as at the UHF level; that is, conformation **B** is in fact the transition state structure for automerization with an activation energy of 14.64 kcal/mol.

Model Dependencies on Geometries and Comparison to Experimental Data. Structures **B** and **C** differ essentially only with respect to the dihedral angles characterizing the rotating CH_2 group. For **B** and **C**, the dihedral angle ∠(H7−C4−2−H8) assumes values between 162° and 171°; that is, in all of the structures *the rotating CH_2 group is only modestly pyramidalized* and resembles the limiting representation **III** more than **IV**. The

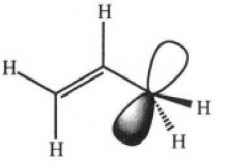

III sp^2

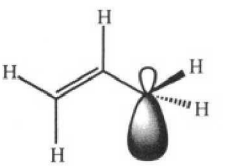

IV sp^3

δ values in Table 3 are the differences between the ∠(H7-C4-C2−H8) angles in **B** and **C**, and they provide a good measure for the similarity between **B** and **C**. All δ values are negative; that is, *the rotating CH_2 groups are more pyramidalized in the **B** than in the **C** structures*. The absolute values $|\delta|$ indicate that the structural differences between **B** and **C** increase in the order $\delta(\text{CISD}) \approx 0 < \delta(\text{CID}) < \delta(\text{CCD}) < \delta(\text{MP2})$. The relative energies of **C** with respect to **B** follow this same order: $\Delta E(\text{CISD}) \approx 0 < \Delta E(\text{CID}) = 0.28 < \Delta E(\text{CCD}) = 0.30 < \Delta E(\text{MP2}) = 0.63$ kcal/mol.

For the C_{2v} structures **A**, all higher levels of theory predict C−C bonds that are shorter (by 0.002−0.014 Å), C−H bonds that are longer (by 0.006−0.013 Å), and decreased ∠(C−C−C) bond angles (0.06−0.14°) compared to the UHF level. All of these changes are very modest. At the best level, QCISD theory predicts d(C−C) = 1.389 Å and ∠(C−C−C) = 124.4°, and we compare these data to the experimental record. The 1986 high-temperature electron diffraction study by Vajda et al.[33] resulted in d(C−C) = 1.428 ± 0.013 Å and ∠(C−C−C) = 124.6 ± 3.4°. While theory and experiment agree excellently with regard to the ∠(C−C−C) angle, the C−C bond length calculated at QCISD level is significantly shorter (by 0.039 Å). This discrepancy may be due to the high temperature of the sample.[34] In 1992, Hirota et al.[35] determined the rotational constants of **A** using infrared diode laser spectroscopy and derived values of d(C−C) = 1.3869 Å and ∠(C−C−C) = 123.96°, and these experimental data are in superb agreement with the QCISD result.

As with **A**, theoretical model dependencies on the C_s structures **B** are modest and of about the same magnitude. Compared to the UHF level, d(C−H) increases by 0.005−0.013 Å at the higher levels, d(C−C) becomes slightly shorter (0.004 Å), and the ∠(C−C−C) changes are much less than 0.5°. Dynamic electron correlation affects the C=C bonds more than the C−C bonds, and there is a qualitative and significant (*vide infra*) difference in the way d(C=C) is affected by the various correlated methods. With respect to the UHF data, the C=C bond is longer at the QCISD level by 0.009 Å, while d(C=C) decreases (0.014−0.022 Å) at the other correlated levels.

The structural relaxation along the rotational automerization pathway affects primarily the CC bonds. The CC bonds in **A** are 1.389 Å, and in **B** they become d(C=C) = 1.313 Å and d(C−C) = 1.477 Å. Note that d(C=C) is shorter than in ethene (1.330 Å), while the value for the $C_{sp^2}-C_{sp^2}$ single bond is as expected. The ∠(C3−C2−C4) angle remains essentially invariant. A small but significant change occurs for the difference ϵ = ∠(H1−C2−C3) − ∠(H1−C2−C4). The ϵ

value reflects different C=C bond strengths in the **B** structures; it is below 2° at UHF and QCISD but above 2° at the other correlated levels.

Vibrational Mode Analysis and Zero-Point Energy Corrections. The ESR experiment shows the rotational barrier in allyl radical to be 15.7 ± 1.0 kcal/mol. UHF theory overestimates with E_{act} = 18.57 kcal/mol, and the removal of the spin contaminations increases E_{act}(PUHF) = 25.33 kcal/mol even further. All other methods give E_{act} values that are within 3 kcal/mol of the experimental value. MP2 and CCD underestimate the barrier somewhat with E_{act} values (**A** versus **C**) of 12.70 and 13.23 kcal/mol, respectively, and so does CID, with E_{act} = 14.30 kcal/mol. Both the CISD (E_{act} = 15.12) and QCISD (E_{act} = 14.64) methods result in activation energies within the standard deviation of the experimental value.

The activation energies E_{act} are determined for the motionless state at absolute zero. A better approximation to the rotational barrier can be obtained by correcting the E_{act} value for the vibrational zero-point energy differences between the minimum and the transition state structure. Contributions by other thermal motions and electronic excitations as well as the T-dependence of changes of the partition functions are small and certainly much smaller than the inherent accuracy of the computations. Thus, we computed the vibrational frequencies for all stationary structures, they are listed in Table 4, and the resulting vibrational zero-point energies are included in Table 1. Vibrational analyses have been the subject of several theoretical studies at different levels of theory,[36] and the IR and Raman spectra have been measured.[9,10] The experimental results are included in Table 4 for comparison, and the agreement is generally good.

The UHF vibrational frequencies are known to be overestimated, and after scaling (factor 0.9) we find that ΔVZPE(**B**,**A**), defined as VZPE(**B**) − VZPE(**A**), is −0.82 kcal/mol. At the QCISD level, ΔVZPE(**B**,**A**) becomes −0.72 kcal/mol, and it is in close agreement. Thus, at the levels QCISD and UHF the estimates for the rotational barriers are 14.65 and 17.75 kcal/mol, respectively. The QCISD estimate is at the low end of the experimental range, and UHF theory overestimates the barrier by about 2 kcal/mol.

Completely unexpected are the ΔVZPE(**C**,**A**) values, defined as VZPE(**C**) − VZPE(**A**), for those methods that indicate **C** as the apparent transition state structure: The ΔVZPE(**C**,**A**) values are +0.16 (MP2), +0.21 (CID), +0.17 (CCD), and +0.22 (CISD); that is, *they all are positive*. In the transition state, one vibration becomes the transition vector and no longer contributes to VZPE. The remaining vibrations should contribute less because the bonding and hence the force constants are reduced in less stable species. To understand this puzzling artifact, we analyzed the normal modes graphically with the program VIBRATE.[37] Unusual vibrational properties are found for the **B** conformations at these levels. QCISD theory predicts ν = 1760 cm^{-1} for the C=C stretching mode in **B**, and the scaled UHF value (1534 cm^{-1}) is significantly lower. The C—C single bond stretching modes occur at 1134 cm^{-1} (QCISD) and 1066 cm^{-1} (UHF, scaled), respectively. *The C=C stretching mode is predicted, erroneously, to be dramatically different at the MP2, CID, CCD, and CISD levels with 2670 cm^{-1} > ν(C=C) > 2230 cm^{-1}*, while ν(C—C) is predicted reasonably well (1161 cm^{-1} > ν(C—C) > 1145 cm^{-1}). This finding corroborates the above structural evidence and underscores in a compelling fashion that the deficiencies associated with these methods are likely to have their *origin in the electron density distributions of the ethene part of allyl radical in conformation **B***. Electron and spin density analyses will show that this conclusion is indeed correct, and we will establish the underlying reason for these deficiencies.

TABLE 4: Vibrational Frequencies of Ally Radical in Conformations A, B, and C[a]

UHF	MP2	CID	CCD	CISD	QCISD	exptl[9c]	exptl[9b]
			A				
451.4	442.6	445.2	440.2	442.7	433.4		
546.7	563.8	558.1	554.6	554.0	534.6	511	510
571.5	591.9	584.0	580.2	579.0	555.6		
779.1	807.5	803.1	796.3	792.2	758.4		
798.3	826.4	821.9	813.8	809.8	772.9	802	801
1004.4	970.3	978.1	963.3	974.6	955.9		
1034.1	1061.3	1048.2	1038.5	1039.2	998.6	985	983
1074.6	1084.5	1082.8	1073.1	1077.9	1055.3		
1250.4	1172.7	1198.3	1175.5	1206.3	1209.0		1184
1341.6	1334.9	1334.0	1321.7	1328.1	1300.4	1242	1242
1536.9	1457.7	1478.1	1452.2	1475.6	1449.2	1389	1389
1637.3	1547.7	1568.0	1538.0	1567.0	1541.5	1463	1463
1647.2	1586.8	1597.4	1572.9	1592.4	1558.4	1477	1477
3327.4	3226.1	3251.3	3190.4	3242.4	3174.9	3016	3019
3327.6	3231.7	3255.5	3197.3	3246.5	3179.4	3016	
3338.5	3239.0	3265.3	3205.3	3256.5	3187.2	3048	3051
3420.3	3338.8	3355.2	3296.0	3345.0	3276.2	3105	3107
3424.1	3340.6	3357.8	3298.4	3347.7	3278.9	3105	3107
			B				
−425.3	382.8	236.0	326.2	106.0	−341.1		
369.9	386.8	375.7	374.5	374.8	366.4		
517.3	527.2	520.0	517.2	517.7	504.4		
601.4	638.5	624.6	625.2	615.7	569.8		
1008.6	1008.6	1015.2	1001.6	1010.6	958.3		
1051.1	1080.9	1077.0	1067.0	1064.0	981.7		
1068.9	1115.5	1108.7	1100.3	1097.0	1018.9		
1136.9	1147.9	1160.9	1144.5	1153.0	1068.2		
1183.6	1195.2	1171.6	1169.7	1157.1	1133.8		
1385.3	1394.5	1414.2	1391.9	1407.8	1352.7		
1547.0	1507.1	1521.2	1495.3	1516.9	1476.3		
1591.5	1533.3	1548.8	1522.3	1544.1	1509.0		
1703.7	2669.8	2384.6	2514.2	2230.4	1760.2		
3279.1	3186.2	3213.9	3153.7	3202.8	3121.3		
3300.1	3245.8	3263.2	3209.1	3251.5	3177.0		
3328.4	3285.8	3280.9	3234.0	3264.5	3180.2		
3393.7	3314.5	3338.2	3274.9	3330.4	3261.3		
3409.8	3356.8	3364.7	3312.0	3351.2	3273.5		
			C				
	−456.7	−312.6	−400.0	−152.7			
	348.2	370.9	357.9	374.9			
	487.6	505.4	487.9	515.1			
	642.2	627.9	628.6	616.4			
	1003.3	1012.9	997.2	1010.2			
	1068.2	1075.6	1058.8	1064.5			
	1109.6	1102.7	1090.3	1095.1			
	1175.0	1161.2	1151.2	1150.0			
	1179.2	1174.2	1164.5	1160.4			
	1392.0	1411.6	1388.1	1407.2			
	1504.7	1520.0	1493.0	1516.7			
	1530.5	1547.4	1519.8	1543.9			
	2157.3	2173.2	2131.8	2184.6			
	3188.2	3212.9	3153.9	3201.5			
	3237.7	3262.0	3205.8	3250.8			
	3248.1	3268.2	3208.9	3261.3			
	3314.8	3336.8	3274.8	3329.0			
	3358.5	3364.2	3311.9	3350.7			

[a] Deviations from standard convergence criteria (not reoptimized because of shallow PES): **B** at CCD, max displ 0.002 964 (0.001 800); **B** at CID, max displ 0.004 939; rms displ 0.001 461 (0.001 200); **C** at CCD, max displ 0.006 849; rms displ 0.018 57; **C** at MP2, max displ 0.001 897.

Another problem with the VZPE corrections relates to ΔVZPE(**C**,**B**). **B** and **C** are structurally very similar and so are the force constants and the associated vibrational frequencies (Table 6). Yet, for **B** the lowest vibrational frequency is positive and included in VZPE(**B**), while the lowest frequency for **C** is imaginary and omitted in the computation of VZPE(**C**). VZPE(**B**) is greater than VZPE(**C**) for this reason, and the calculated differences are so large as to indicate a reversal of the relative stability of **B** and **C** if the ΔVZPE(**C**,**B**) values were applied.

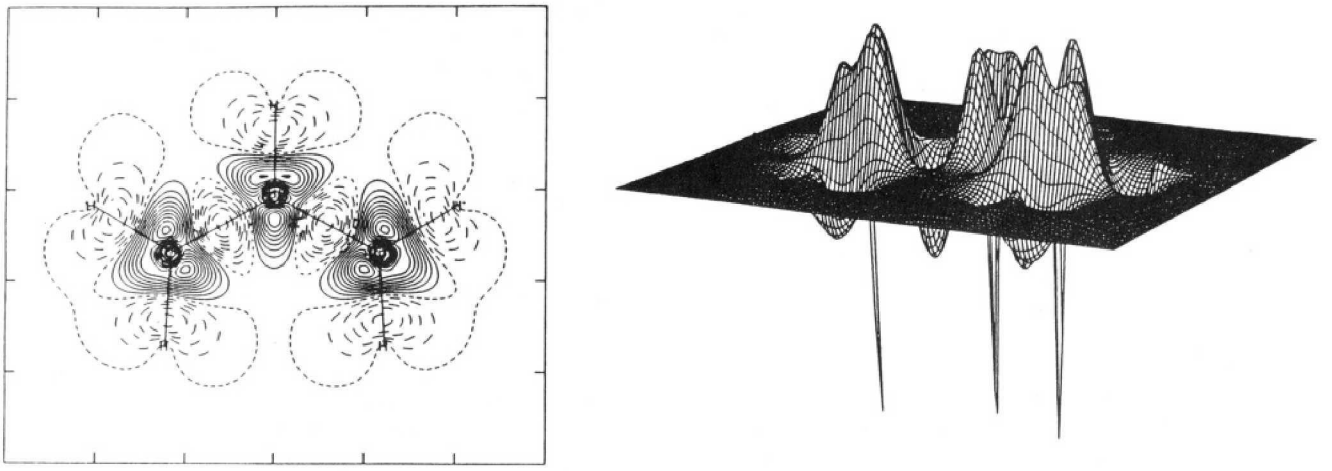

Figure 2. Contour plots of the electron density difference function $\Delta\varrho = \varrho(\text{QCISD}) - \varrho(\text{UHF})$ of allyl radical **A** in the molecular plane (left). Positive areas $\Delta\varrho$ are contoured with solid lines, short-dashed lines indicate $\Delta\varrho = 0$, and long-dashed lines contour negative regions of $\Delta\varrho$. Contours are shown with increments of 10^{-3} e au^{-3}. The surface plot on the right (logarithmic scale) illustrates $\Delta\varrho$ in the immediate vicinity of the nuclei.

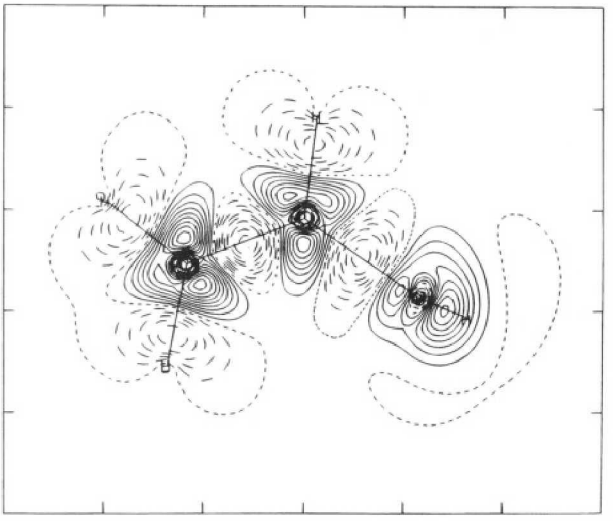

Figure 3. Electron density difference function $\Delta\varrho = \varrho(\text{QCISD}) - \varrho(\text{UHF})$ of allyl radical in conformation **B** in the symmetry plane. The increment settings are as in Figure 2.

This conclusion cannot be drawn, however, since the lowest frequencies also are the Least accurate and because ΔVZPE-(**C**,**B**) is dominated by the term $h[\nu_1^{\text{imag}}(\mathbf{B}) - \nu_1(\mathbf{C})]$ since the terms $h[\nu_i(\mathbf{B}) - \nu_i(\mathbf{C})]$ are small for all other respective frequencies (Table 4).

Electron Density and Spin Density Analysis. Topological electron density and spin density analyses were carried out at all theoretical levels for **A** and **B** to investigate electron correlation effects. The electron density ϱ and the spin density ϱ^S are the sum or difference, respectively, of the α and β electron density functions.

electron density: $$\varrho = \varrho_\alpha + \varrho_\beta$$

spin density: $$\varrho^S = \varrho_\alpha - \varrho_\beta$$

Electron density difference functions (EDD) are defined as the difference between the electron density functions ϱ(Method1) and ϱ(Method2), and spin density difference functions are defined in analogy. Here we will use ϱ(UHF) as the reference:

$$\Delta\varrho(\text{Method1} - \text{UHF}) = \varrho(\text{Method1}) - \varrho(\text{UHF})$$

$$\Delta\varrho^S(\text{Method1} - \text{UHF}) = \varrho^S(\text{Method1}) - \varrho^S(\text{UHF})$$

The computation of difference functions intrinsically requires the use of one structure, and the UHF structures were used. We have shown previously that the choice of structure is not critical,[2b] and for allyl radical the model-dependent structure variations are indeed very small.

Topological properties of the electron densities are summarized in Table 5. Integrated properties are collected in Table 4, and values are given for the integrated electron populations (IP) and the integrated spin populations (SP) determined for **A** and **B** at each level on the basis of the structures optimized at each level. For clarity, the ΔIP(**A**,**B**) and ΔSP(**A**,**B**) values given

$$\Delta\text{IP}(\mathbf{A},\mathbf{B}) = \text{IP}(\mathbf{A}) - \text{IP}(\mathbf{B})$$

$$\Delta\text{SP}(\mathbf{A},\mathbf{B}) = \text{SP}(\mathbf{A}) - \text{SP}(\mathbf{B})$$

are the changes for each of these properties depending on conformation. The discussion of the theoretical model dependency is facilitated by considering relative instead of absolute data. The ΔIP^M and ΔSP^M parameters used for this purpose are defined as shown with reference to the UHF derived data for conformation **A** and in complete analogy for conformation **B**.

$$\Delta\text{IP}^M(\mathbf{A}) = \text{IP}(\text{Method},\mathbf{A}) - \text{IP}(\text{UHF},\mathbf{A})$$

$$\Delta\text{SP}^M(\mathbf{A}) = \text{SP}(\text{Method},\mathbf{A}) - \text{SP}(\text{UHF},\mathbf{A})$$

Electron Density Difference Functions. Contour plots of the EDD functions $\Delta\varrho$(Method1−UHF) of allyl radical **A** are qualitatively similar at all correlated levels, and, in Figure 2, plots of $\Delta\varrho$(QCISD−UHF) are shown. Both the σ and π electron densities decrease in all C—C and C—H bonds, while electron density increases occur close to the nuclei. These electron correlation effects are consistent with excitations from bonding to antibonding MOs. Note that the $\Delta\varrho$ maxima in the C regions occur "behind" the C atoms with respect to their bonds. Electron correlation effects in the immediate proximity of the nuclei are not readily discernible from the contour plots, but the surface plot shown in Figure 2 demonstrates well that correlation dramatically reduces the electron density in the immediate vicinity of the C nuclei.

As with **A**, contour plots of the $\Delta\varrho$ functions in the symmetry plane of the **B** structures are qualitatively similar, and $\Delta\varrho$-(QCISD−UHF) is shown in Figure 3 as an example. The pattern in the "ethene" part resembles the features found and discussed for **A** (Figure 2). Significantly more method-dependent variations are manifested in the cross sections

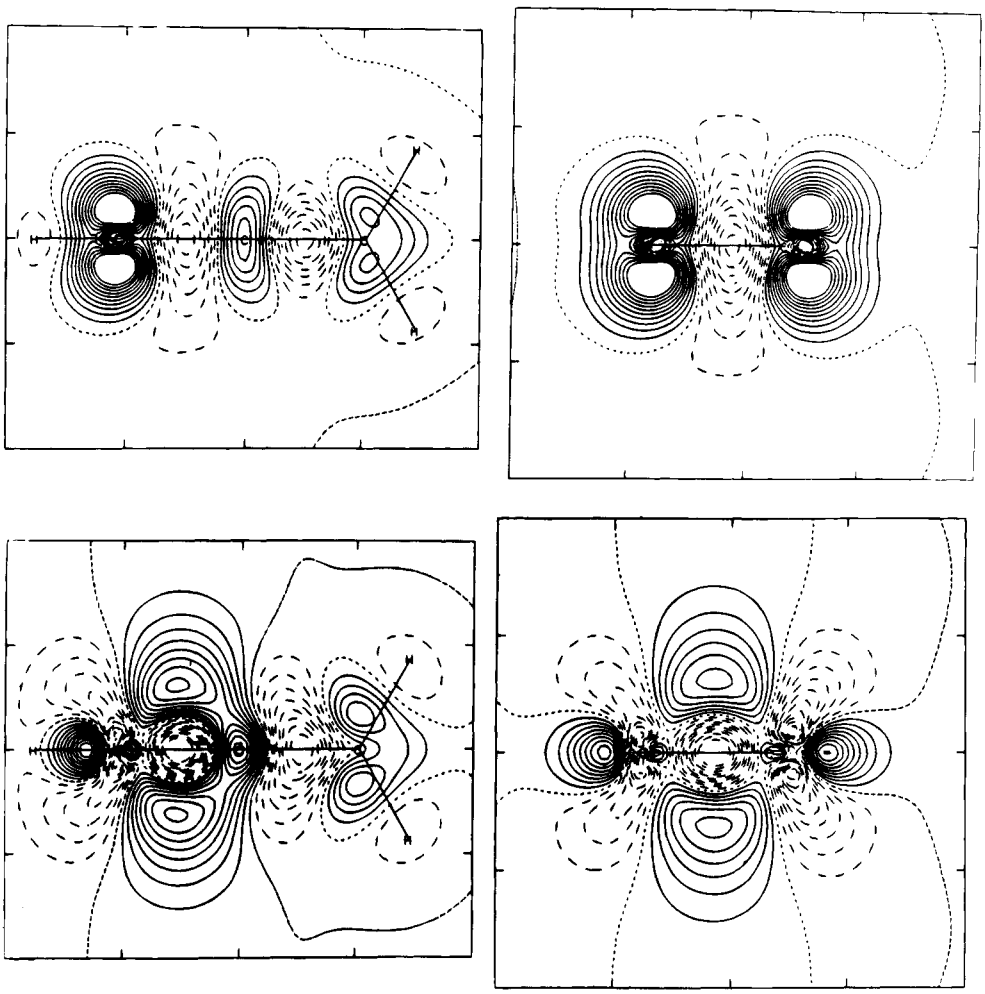

Figure 4. Electron density difference functions $\Delta\varrho = \varrho(\text{Method1}) - \varrho(\text{UHF})$ of allyl radical in its **B** conformation as determined for the methods QCISD (top row) and MP2 (bottom row). Plots on the left are cross sections that contain the rotating CH_2 group, and the plots on the right show cross sections that are perpendicular to the molecular plane and contain the C=C bond C atoms. Contour increments are 10^{-3} e au^{-3} in all cases.

computed for planes that are orthogonal to the molecular plane. Two such planes were examined. To the left in Figure 4, cross sections are shown for the planes that contain the atoms of the rotating CH_2 group for the functions $\Delta\varrho$(QCISD−UHF) and $\Delta\varrho$(MP2−UHF), and the cross sections on the right show the plane containing the C atoms of the ethene part at the same levels. The respective plots of $\Delta\varrho$(CISD−UHF), $\Delta\varrho$(CID−UHF), and $\Delta\varrho$(CCD−UHF) also were examined and found to resemble those for $\Delta\varrho$(MP2−UHF). The regions of $\Delta\varrho$ at the rotating CH_2 group are affected comparatively little by the theoretical method. In all cases, correlation causes electron depletion in the C−C bonding region, and electron density increases in a "kidney-shaped" area at the C atom. Method-dependent differences occur in the "ethene" part of **B**. At the best theoretical level, we find a polarization pattern where positive areas of $\Delta\varrho$ occur close to the C atoms of the ethene part and where electron correlation causes density depletion in the π-bonding region. This polarization pattern *is the same* as the one found in the molecular plane (Figure 3). The cross section of $\Delta\varrho$(MP2−UHF) is remarkably different. It is no longer true that a common polarization pattern occurs in these two planes. At the MP2 level, π density is shifted from the C atoms into the π-bonding region. Thus, *while QCISD theory causes σ and π density to be shifted out of the bonding regions and toward the atomic regions, at the MP2, CID, CCD, and CISD levels, we find such σ density shifts, but they are partially offset by shifts in the π system in the opposite direction.*

Topological Analysis and Electron Populations. The electron density functions for **A**−**C** were analyzed topologically, and characteristic properties of the bond critical points are summarized in Table 5. The critical point data were then employed to determine the zero-flux surfaces that define the atomic regions and to determine the integrated atomic properties given in Table 6. We first consider the QCISD data and subsequently compare them to the data obtained at UHF and the other correlated methods.

In **A**, the IP(QCISD) data indicate negative charges of −0.119 and −0.013 for the terminal and central C atoms, respectively, and the H populations are such that the CH_2 and CH groups are assigned overall charges of −0.013 and +0.029.[38] For **B**, the respective IP values indicate negative charges for the C atoms of −0.094 (H_2C=), −0.031 (CH), and −0.140 (−CH_2), and the group charges become +0.001 (H_2C=), +0.013 (CH), and −0.010 (−CH_2). The ΔIP(**A**,**B**) values for the three fragments are −0.014 (H_2C=), 0.016 (CH), and −0.003 (−CH_2). Thus, the overall polarity of allyl radical is marginal. Secondly, there occurs a small shift of electron density toward the central CH group during automerization, and this increase mostly is due to a shift from the CH_2 group of the ethene part.

The IP values and ΔIP(**A**,**B**) values of individual atoms vary modestly depending on the theoretical model (Table 6), and most of these variations are due to the C−H partitioning. Since the ΔIP^M(H) values at all correlated levels decrease by 0.023−0.043 while ΔIP^M(C) values increase by 0.026−0.079, the model dependencies for the group ΔIP(**A**,**B**) values are only marginal. All methods agree that the ΔIP(**A**,**B**) values for the H_2C= and H_2C− groups are negative while that for the CH group is positive (< 0.032) and that ΔIP(**A**,**B**) for the rotating CH_2 group

TABLE 5: Topological Properties of the Various Conformations of Allyl Radical

method[a]	r_A	r_B	R	ϱ	λ_1	λ_2	λ_3	ϵ
				A				
QCISD								
H1–C2	0.389	0.701	0.357	0.273	−0.734	−0.724	0.516	0.013
C2–C3	0.696	0.694	0.501	0.313	−0.653	−0.525	0.311	0.243
C3–H5	0.700	0.387	0.644	0.272	−0.731	−0.712	0.510	0.026
C3–H6	0.699	0.386	0.644	0.274	−0.738	−0.716	0.510	0.028
CISD								
H1–C2	0.389	0.696	0.359	0.278	−0.749	−0.740	0.505	0.012
C2–C3	0.693	0.690	0.501	0.318	−0.672	−0.537	0.297	0.250
C3–H5	0.695	0.387	0.642	0.277	−0.746	−0.727	0.498	0.025
C3–H6	0.695	0.386	0.643	0.279	−0.752	−0.732	0.498	0.028
CCD								
H1–C2	0.389	0.701	0.357	0.274	−0.738	−0.730	0.517	0.010
C2–C3	0.692	0.689	0.501	0.318	−0.668	−0.534	0.304	0.251
C3–H5	0.700	0.387	0.644	0.274	−0.735	−0.718	0.510	0.023
C3–H6	0.699	0.386	0.645	0.275	−0.742	−0.723	0.510	0.026
CID								
H1–C2	0.389	0.696	0.358	0.279	−0.752	−0.743	0.506	0.011
C2–C3	0.691	0.688	0.501	0.320	−0.677	−0.542	0.295	0.251
C3–H5	0.695	0.387	0.642	0.278	−0.748	−0.730	0.499	0.025
C3–H6	0.694	0.386	0.643	0.279	−0.755	−0.735	0.498	0.027
MP2								
H1–C2	0.385	0.703	0.354	0.276	−0.744	−0.739	0.506	0.007
C2–C3	0.690	0.686	0.502	0.320	−0.670	−0.535	0.301	0.254
C3–H5	0.701	0.383	0.647	0.275	−0.743	−0.727	0.498	0.022
C3–H6	0.700	0.382	0.647	0.277	−0.750	−0.733	0.498	0.024
PUHF								
H1–C2	0.394	0.683	0.366	0.287	−0.772	−0.761	0.467	0.015
C2–C3	0.696	0.694	0.501	0.320	−0.688	−0.545	0.265	0.262
C3–H5	0.683	0.392	0.635	0.285	−0.766	−0.744	0.461	0.030
C3–H6	0.682	0.391	0.636	0.286	−0.772	−0.748	0.461	0.032
UHF								
H1–C2	0.394	0.683	0.366	0.288	−0.772	−0.758	0.467	0.018
C2–C3	0.696	0.694	0.501	0.320	−0.688	−0.551	0.266	0.248
C3–H5	0.683	0.393	0.635	0.285	−0.766	−0.742	0.462	0.031
C3–H6	0.682	0.391	0.635	0.286	−0.772	−0.747	0.462	0.034
				B				
QCISD								
H1–C2	0.391	0.704	0.357	0.269	−0.717	−0.704	0.514	0.017
C2–C3	0.672	0.663	0.504	0.341	−0.736	−0.518	0.265	0.420
C2–C4	0.736	0.470	0.499	0.269	−0.516	−0.500	0.333	0.031
C3–H5	0.700	0.388	0.644	0.273	−0.733	−0.722	0.511	0.016
C3–H6	0.699	0.388	0.643	0.273	−0.733	−0.721	0.510	0.016
C4–H7	0.701	0.386	0.645	0.271	−0.728	−0.699	0.508	0.041
CISD								
H1–C2	0.391	0.699	0.359	0.275	−0.736	−0.728	0.504	0.011
C2–C3	0.664	0.647	0.506	0.359	−0.791	−0.532	0.223	0.488
C2–C4	0.738	0.378	0.500	0.271	−0.527	−0.509	0.324	0.036
C3–H5	0.696	0.387	0.642	0.278	−0.749	−0.742	0.500	0.010
C3–H6	0.694	0.388	0.641	0.278	−0.748	−0.741	0.499	0.010
C4–H7	0.696	0.385	0.644	0.276	−0.744	−0.715	0.496	0.041
CCD								
H1–C2	0.390	0.704	0.356	0.271	−0.725	−0.719	0.515	0.009
C2–C3	0.663	0.645	0.507	0.360	−0.791	−0.526	0.226	0.504
C2–C4	0.739	0.740	0.500	0.269	−0.521	−0.503	0.332	0.037
C3–H5	0.700	0.387	0.644	0.274	−0.737	−0.731	0.512	0.008
C3–H6	0.699	0.388	0.643	0.274	−0.736	−0.730	0.511	0.008
C4–H7	0.701	0.384	0.646	0.273	−0.735	−0.707	0.507	0.040
CID								
H1–C2	0.390	0.698	0.359	0.276	−0.739	−0.732	0.504	0.010
C2–C3	0.663	0.644	0.507	0.362	−0.801	−0.534	0.216	0.498
C2–C4	0.737	0.738	0.500	0.272	−0.530	−0.511	0.323	0.036
C3–H5	0.695	0.387	0.642	0.279	−0.751	−0.745	0.500	0.009
C3–H6	0.697	0.388	0.643	0.279	−0.750	−0.743	0.499	0.009
C4–H7	0.696	0.309	0.692	0.277	−0.747	−0.717	0.496	0.041
MP2								
H1–C2	0.387	0.705	0.354	0.272	−0.729	−0.725	0.503	0.006
C2–C3	0.662	0.643	0.507	0.360	−0.788	−0.521	0.226	0.513
C2–C4	0.738	0.736	0.501	0.270	−0.524	−0.505	0.328	0.037
C3–H5	0.701	0.383	0.647	0.276	−0.744	−0.739	0.500	0.006
C3–H6	0.700	0.385	0.646	0.276	−0.743	−0.738	0.499	0.007
C4–H7	0.701	0.381	0.648	0.275	−0.743	−0.717	0.494	0.037
PUHF								
H1–C2	0.395	0.686	0.365	0.283	−0.759	−0.746	0.469	0.016
C2–C3	0.670	0.656	0.505	0.357	−0.800	−0.550	0.203	0.455
C2–C4	0.740	0.739	0.500	0.275	−0.541	−0.524	0.294	0.033
C3–H5	0.684	0.392	0.636	0.286	−0.770	−0.758	0.464	0.015
C3–H6	0.683	0.393	0.635	0.286	−0.770	−0.758	0.463	0.016
C4–H7	0.685	0.391	0.637	0.048	−0.760	−0.725	0.462	0.048
UHF								
H1–C2	0.395	0.686	0.365	0.283	−0.758	−0.746	0.469	0.017
C2–C3	0.669	0.657	0.505	0.357	−0.800	−0.554	0.204	0.444
C2–C4	0.740	0.738	0.500	0.275	−0.540	−0.523	0.294	0.032
C3–H5	0.684	0.392	0.636	0.286	−0.770	−0.758	0.464	0.016
C3–H6	0.682	0.393	0.635	0.286	−0.770	−0.758	0.463	0.016
C4–H7	0.685	0.391	0.637	0.282	−0.759	−0.724	0.462	0.048

[a] Parameters r_A and r_B are the distances of the bond critical point (BCP) from the atoms A and B specified in the first column in angstroms; $R = r_A/(r_A + r_B)$; ϱ is the value of the electron density at the BCP (in e au^{-3}), λ_i are the principal curvatures of ϱ at the BCP, and the elipticity is derived via $\epsilon = \lambda_n/\lambda_m - 1$, where $\lambda_n < \lambda_m$ and $\lambda_i < 0$.

TABLE 6: Integrated Electron and Spin Populations of C_{2v} and C_s Allyl Radical

		IP			SP		
method	atom	A	B	ΔIP(A,B)	A	B	ΔSP(A,B)
QCISD	H1	0.958	0.956	0.002	0.000	0.034	−0.034
	C2	6.013	6.031	−0.018	−0.165	0.017	−0.182
	C3	6.119	6.094	0.025	0.589	−0.002	0.591
	C4		6.140	−0.021		0.950	−0.361
	H5	0.949	0.951	−0.002	−0.003	0.003	−0.006
	H6	0.945	0.954	−0.009	−0.003	0.004	−0.007
	H7		0.935	0.010		−0.003	0.000
	=CH_2	−0.013	0.001	−0.014	0.583	0.005	0.578
	CH	0.029	0.013	0.016	−0.165	0.051	−0.216
	−CH_2		−0.010	−0.003		0.944	−0.361
CISD	H1	0.965	0.962	0.003	0.001	0.026	−0.025
	C2	6.006	6.034	−0.028	−0.244	0.338	−0.582
	C3	6.107	6.076	0.031	0.631	−0.346	0.977
	C4		6.128	−0.021		0.950	−0.319
	H5	0.955	0.958	−0.003	−0.005	0.010	−0.015
	H6	0.952	0.962	−0.010	−0.004	0.010	−0.014
	H7		0.939	0.013		0.005	−0.009
	=CH_2	−0.014	0.004	−0.018	0.622	−0.326	0.948
	CH	0.029	0.004	0.025	−0.243	0.364	−0.607
	−CH_2		−0.006	−0.008		0.960	−0.338
CCD	H1	0.958	0.955	0.003	−0.004	0.017	−0.021
	C2	6.013	6.043	−0.030	−0.187	0.639	−0.826
	C3	6.122	6.088	0.034	0.596	−0.660	1.256
	C4		6.142	−0.020		0.926	−0.330
	H5	0.948	0.951	−0.003	0.000	0.019	−0.019
	H6	0.944	0.953	−0.009	0.000	0.019	−0.019
	H7		0.932	0.012		0.020	−0.020
	=CH_2	−0.014	0.008	−0.022	0.596	−0.622	1.218
	CH	0.029	0.002	0.027	−0.191	0.656	−0.847
	−CH_2		−0.006	−0.008		0.966	−0.370
CID	H1	0.965	0.962	0.003	−0.001	0.022	−0.023
	C2	6.007	6.036	−0.029	−0.247	0.458	−0.705
	C3	6.109	6.076	0.033	0.631	−0.472	1.103
	C4		6.129	−0.020		0.943	−0.312
	H5	0.954	0.957	−0.003	−0.004	0.013	−0.017
	H6	0.951	0.960	−0.009	−0.003	0.014	−0.017
	H7		0.939	0.012		0.011	−0.014
	=CH_2	−0.014	0.007	−0.021	0.624	−0.445	1.069
	CH	0.028	0.002	0.026	−0.248	0.480	−0.728
	−CH_2		−0.007	−0.007		0.965	−0.341
MP2	H1	0.95	0.948	0.002	−0.004	0.016	−0.020
	C2	6.021	6.055	−0.034	−0.159	0.797	−0.956
	C3	6.135	6.103	0.032	0.585	−0.825	1.410
	C4		6.151	−0.016		0.923	−0.338
	H5	0.942	0.943	−0.001	−0.002	0.021	−0.023
	H6	0.938	0.946	−0.008	−0.002	0.022	−0.024
	H7		0.927	0.011		0.023	−0.025
	=CH_2	−0.015	0.008	−0.023	0.581	−0.782	1.363
	CH	0.029	−0.003	0.032	−0.163	0.813	−0.976
	−CH_2		−0.005	−0.010		0.969	−0.388
PUHF	H1	0.992	0.989	0.003	0.004	0.027	−0.023
	C2	5.976	6.004	−0.028	−0.110	−0.064	−0.046
	C3	6.057	6.032	0.025	0.543	0.112	0.431
	C4		6.074	−0.017		0.904	−0.361
	H5	0.981	0.982	−0.001	0.005	0.000	0.005
	H6	0.977	0.984	−0.007	0.005	0.000	0.005
	H7		0.966	0.011		0.010	−0.005
	=CH_2	−0.015	0.002	−0.017	0.553	0.112	0.441
	CH	0.032	0.007	0.025	−0.106	−0.037	−0.069
	−CH_2		−0.006	−0.009		0.924	−0.371
UHF	H1	0.993	0.988	0.005	0.009	0.040	−0.031
	C2	5.979	6.005	−0.026	−0.449	−0.275	−0.174
	C3	6.056	6.032	0.024	0.748	0.282	0.466
	C4		6.071	−0.015		1.011	−0.263
	H5	0.981	0.982	−0.001	−0.013	−0.004	−0.009
	H6	0.978	0.985	−0.007	−0.014	−0.003	−0.011
	H7		0.966	0.012		−0.026	0.012
	=CH_2	−0.015	0.001	−0.016	0.721	0.275	0.446
	CH	0.028	0.007	0.021	−0.440	−0.235	−0.205
	−CH_2		−0.003	−0.012		0.959	−0.238

is less negative than for the H_2C= group. *All methods predict the same type of electron density relaxation along the automerization path.*

Spin Density Functions and Spin Density Difference Functions. The SD functions computed for conformation **A** at the various levels are qualitatively similar, and the plot of ϱ^S(QCISD) is shown in Figure 5. The terminal C atoms carry α-spin as expected on the basis of the nodal properties of the π HOMO, spin polarization causes β-spin accumulation at the central C atom, and ϱ^S(QCISD) changes sign along each C−H bond.

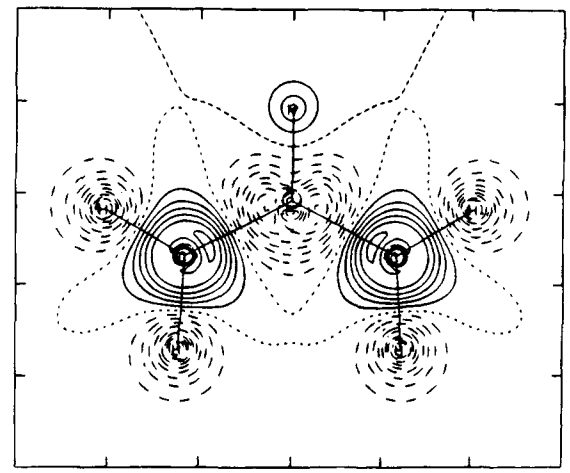

Figure 5. Spin density function ϱ^S(QCISD) of allyl radical **A** in the molecular plane. Contour increments are 10^{-3} α-e au^{-3}.

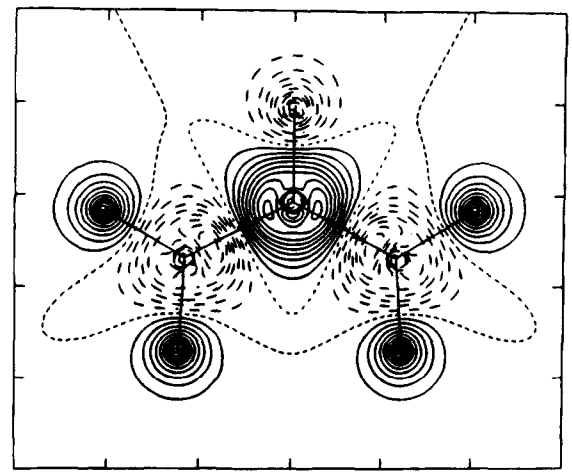

Figure 6. Spin density difference function $\Delta\varrho^S = \varrho^S$(QCISD) − ϱ^S(UHF) of allyl radical **A** in the molecular plane. Contour increments are 10^{-3} α-e au^{-3}.

We reported previously for representative series of radicals, including allyl radical, that annihilation of unwanted spin states via projection (PUHF) decreases spin polarization compared to UHF theory.[2a] More recently, we found that electron correlation in general also reduces spin polarization for $^{\cdot}XH_n$ radicals,[2b] and the present work shows that this also is true for allyl radical. The function $\Delta\varrho^S$(QCISD−UHF) is shown in Figure 6, and it is representative of all $\Delta\varrho^S$ functions.

The SDD functions $\Delta\varrho^S$(QCISD−PUHF), $\Delta\varrho^S$(CISD−PUHF), $\Delta\varrho^S$(CID−PUHF), $\Delta\varrho^S$(CCD−PUHF), and $\Delta\varrho^S$(MP2−PUHF) are shown in Figure 7 for **A**. Comparison between $\Delta\varrho^S$(QCISD−PUHF) and $\Delta\varrho^S$(QCISD−UHF) shown in Figure 6 reveals that QCISD theory results in spin polarizations that are intermediate between those predicted at the UHF and PUHF levels with one exception. For the H atom in the central position, both of the $\Delta\varrho^S$ functions are negative and QCISD predicts less α-spin excess for this atom than at UHF or PUHF.

The plots of the $\Delta\varrho^S$ functions for QCISD, CISD, and CID are all qualitatively similar, and they differ only slightly in the region of the central C−H bond. More drastic differences do occur for the $\Delta\varrho^S$ functions of the CCD and MP2 densities. While the terminal-H regions of $\Delta\varrho^S$(CCD−PUHF) and $\Delta\varrho^S$-

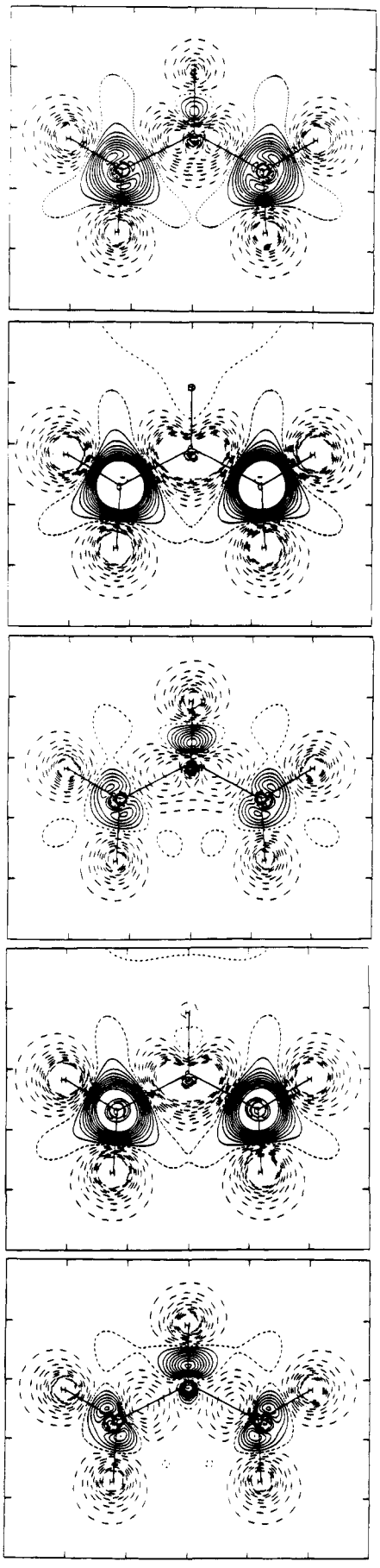

Figure 7. Spin density difference functions $\Delta\varrho^S$(Method1−PUHF) of allyl radical **A** in the molecular plane, where "Method1" refers to the levels (top to bottom) QCISD, CISD, CCD, CID, and MP2. Contour increments are 2×10^{-3} α-e au^{-3}.

(MP2−PUHF) greatly resemble those in $\Delta\varrho^S$(QCISD−PUHF), the former $\Delta\varrho^S$ functions show a much lower contour density at the C atoms compared to $\Delta\varrho^S$(QCISD−PUHF). This indicates that the spin densities at the terminal C atoms computed at these levels are reduced more than at the QCISD level and that they resemble those obtained at the PUHF level more closely. The other significant difference relates to the occurrence of a pronounced area in the central C−H bonding region where the functions $\Delta\varrho^S$(CCD−PUHF) and $\Delta\varrho^S$(MP2−PUHF) are positive. Such an area is missing in the plots of $\Delta\varrho^S$(CISD−PUHF) and $\Delta\varrho^S$(CID−PUHF), and there is only a very small indication of this feature found for $\Delta\varrho^S$(QCISD−PUHF).

For **A**, we find that spin polarization is reduced at all correlated levels in comparison to the UHF level and that it is intermediate between the spin polarizations predicted with the UHF and PUHF densities (with the one discussed exception of H_{cent}). At the MP2 and CCD levels, the reduction in spin polarization is more pronounced for the C−C bonds compared to the other correlated levels, while these methods result in about the same changes to the spin density functions for the C−H bonds of the CH_2 groups.

For conformation **B**, the functions ϱ^S(UHF) and ϱ^S(PUHF) are qualitatively similar and contour plots of ϱ^S(PUHF) are shown in Figure 8. In **B**, the delocalization of the unpaired electron is very much reduced, but significant spin polarization in the ethene part does occur. Note that the central H atom has significantly more α-spin in **B** than in **A**. The inclusion of electron correlation at our highest level, QCISD, results in a remarkably similar ϱ^S function. The only significant qualitative difference relates to the small α-spin excess at the in-plane methylene H atoms in contrast to the small β-spin excess found at the UHF levels.

Major differences occur at the other correlated levels. The SD function characteristics found at the MP2 and CCD levels and at the CID and CISD levels, respectively, are similar, and only contour plots of ϱ^S(CCD) and ϱ^S(CISD) are illustrated. The great similarity between the CID and CISD functions was not expected; but we find for **B** that the CISD single excitations do not have any significant effect on the spin density distribution. Most importantly, *it is found that the spin polarizations at all atoms of the H_2C=CH− fragment are reversed at the MP2, CCD, CID, and CISD levels compared to the UHF and PUHF levels!* At the CISD level, the spin polarization within the in-plane CH_2 group is of the same type as for the other levels but reduced in magnitude. The major difference between ϱ^S(CISD) compared to the CCD and MP2 ϱ^S functions occurs in the central CH region where CISD indicates a pronounced shift of excess α-density from C to H.

While the changes in the H_2C=CH− fragment can be well characterized by analysis of the spin density functions, the analysis of the theoretical model dependencies on the spin density function at the rotating CH_2 group requires the consideration of SDD functions. Three of these are shown in Figure 9. The respective $\Delta\varrho^S$ functions of MP2, CID, and CCD produce similar patterns as found for $\Delta\varrho^S = \varrho^S$(CISD) − ϱ^S(PUHF). The two plots shown on top and in the center of Figure 9 show again that QCISD theory reduces the spin polarization compared to the HF level and that the QCISD spin density resembles the PUHF density more than the UHF density. Compared to the UHF level, QCISD removes excess α-spin in a spherical region from the rotating C atom. The differences between the QCISD and PUHF densities are generally less, and there are more anisotropic features. The spin density in the in-plane p orbital at the rotating C atom is more diffuse at the QCISD level than at PUHF and anisotropic effects also can be

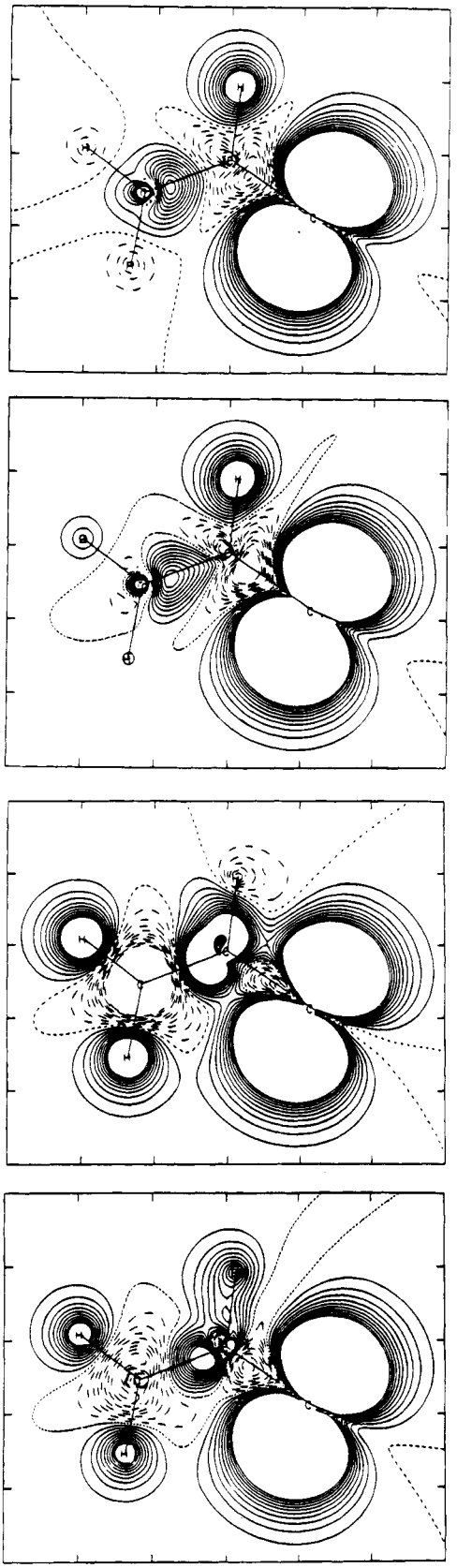

Figure 8. Spin density functions (from the top down) ϱ^S(PUHF), ϱ^S(QCISD), ϱ^S(CCD), and ϱ^S(CISD) of allyl radical **B** in the molecular plane. Contour increments are 0.7×10^{-3} α-e au^{-3}.

seen at the position of the central C atom. The difference function $\Delta\varrho^S = \varrho^S(\text{CISD}) - \varrho^S(\text{PUHF})$ shows a larger p-shaped positive area at the rotating CH_2, indicating an overestimated α-spin concentration at that location, while an underestimation of β-spin at C_{cent} (positive area) occurs at the same time.

We have shown above that electron correlation always reduces the electron density in the C—C bonding regions but that the mechanisms by which this electron depletion is accomplished may differ depending on the method. No such method dependencies occur in the SDD functions. The cross sections of the $\Delta\varrho^S$ functions in the orthogonal plane containing the C=C bond show the same pattern (Figure 9, right) irrespective of the method.

Spin Populations. We will discuss the spin populations for the three CH_n fragments (Table 6) first and then briefly consider the individual SP(H) data. The spin populations for the CH_2 and CH fragments of **A** reflect and quantify the spin polarization seen in the spin density functions. At the QCISD level, the CH_2 groups have SP values in excess of 0.5 α-e and the CH group carries 0.165 units β-spin. SP(CH_2) and SP(CH) are 0.721 and −0.440 at the UHF level, and they are overestimated, as suggested by the SDD function analysis. Spin annihilation at the PUHF level results in SP(CH_2) and SP(CH) values of 0.553 and −0.106; these values are in much better agreement with the QCISD data while underestimating spin polarization somewhat. The same type of spin polarization occurs at all other levels, and the correlated levels always yield SP values that are improved compared to the UHF level.

In **B**, the unpaired electron becomes localized in the p-shaped MO at the rotating CH_2 group carbon. The QCISD SP values show that the total spin population at the rotating CH_2 group (0.944) is *less than unity* and that there are small amounts of α-spin delocalized over the CH (0.051) and $=CH_2$ (0.005) groups. This situation is significantly different compared to the UHF level. UHF agrees with QCISD theory in that most, but again less than unity, of the α-spin is localized (0.959), but UHF indicates significant spin polarization within the H_2C=CH− group. Spin annihilation reduces the spin polarization within the H_2C=CH− group, SP(CH_2) = 0.112 and SP(CH) = −0.037, but not as completely as does QCISD theory. Nevertheless, there is qualitative agreement between the UHF, PUHF, and QCISD methods, that is, among all the methods that result in the correct potential energy surface characteristics. The other correlated methods also predict spin populations of 0.965 ± 0.0.005 for the rotating CH_2 group, but they all would indicate spin polarizations within the H_2C=CH− fragment that are *much larger than at the UHF level* and *of opposite polarity*. With these methods, localization of the unpaired electron leads to a reversal of the spin polarization within the H_2C=CH− fragment via the spin delocalization mechanism (*vide infra*), and its magnitude increases in the order CISD, CCD, CID, and MP2.

In Figure 10, the values ΔSP^M are plotted for all atoms of allyl radical. Note that the ΔSP^M values can be very large indeed (>1!) and that the magnitude of ΔSP^M is *not* related to the magnitude of the spin population at that atom (e.g. SP(C4) > 0.95 while 0 > ΔSP^M(C4) > −0.2). For **B**, the ΔSP^M(C4) values all are less than 0, and they show little variation; all methods predict an α-spin population at the radical site that is less than unity and lower than at the UHF level. All ΔSP^M-(C2) are positive and all ΔSP^M(C3) are negative for both **A** and **B**. A characteristic difference between **A** and **B** can be seen: For the delocalized allyl radical **A**, the effects of annihilation are larger than the QCISD effects of electron correlation, while the opposite is true for the localized allyl radical **B**. When $|\Delta SP^{PUHF}| > |\Delta SP^{QCISD}|$, the ΔSP^M values for the other methods fall between the values ΔSP^{PUHF} and ΔSP^{QCISD}, and when $|\Delta SP^{PUHF}| < |\Delta SP^{QCISD}|$, then the ΔSP^M values for the other methods are larger in magnitude than ΔSP^{PUHF} and have the same sign. These findings show that the spin polarizations of (delocalized) π radicals are affected less by the deficiencies of the MP2, CID, CCD, and CISD

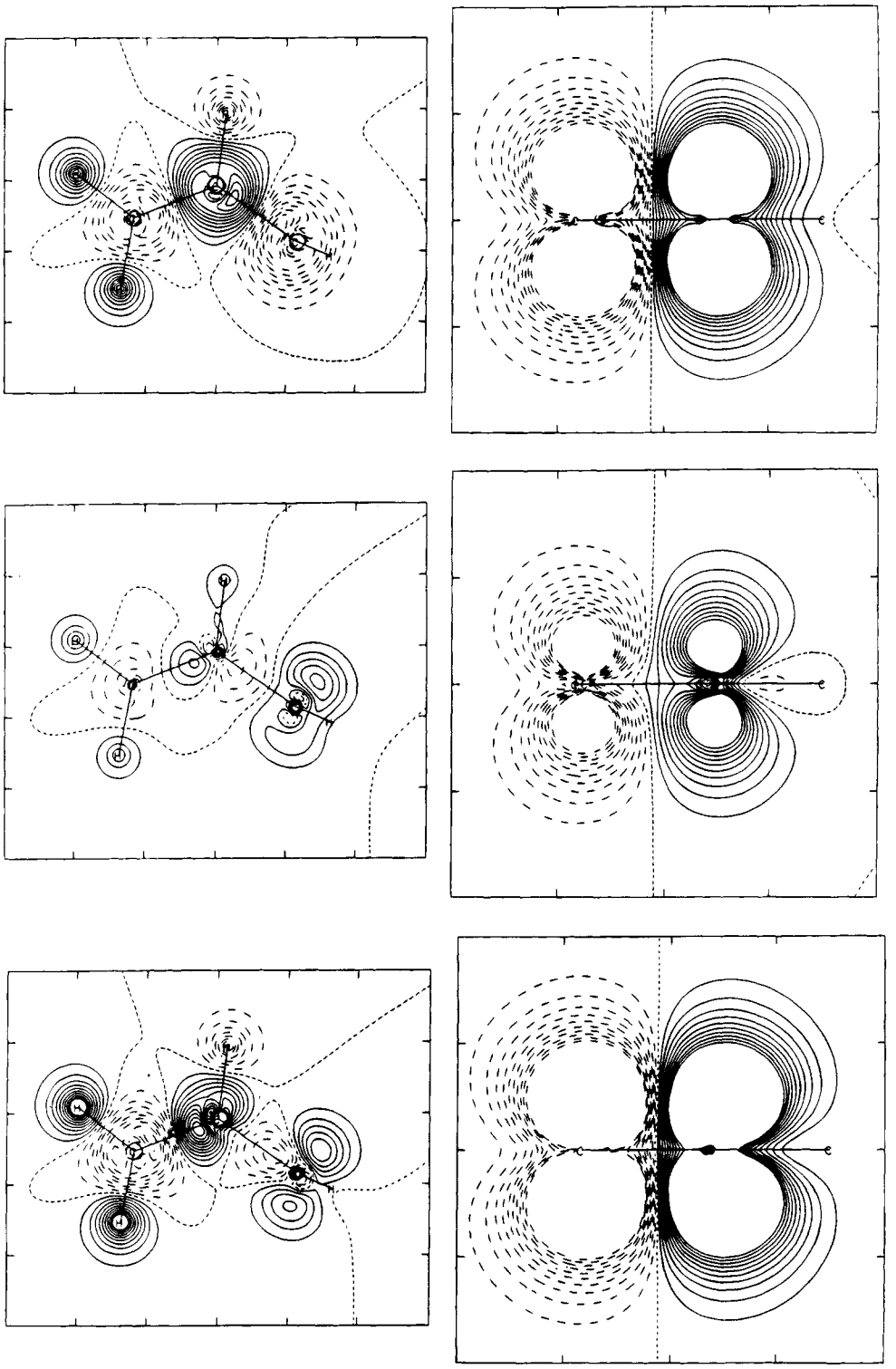

Figure 9. Spin density difference functions $\Delta\varrho^S = \varrho^S(\text{QCISD}) - \varrho^S(\text{UHF})$, $\Delta\varrho^S = \varrho^S(\text{QCISD}) - \varrho^S(\text{PUHF})$, and $\Delta\varrho^S = \varrho^S(\text{CISD}) - \varrho^S(\text{PUHF})$ of allyl radical **B** in the molecular plane (left). The cross sections to the right show the functions in a plane orthogonal to the molecular plane and containing the C atoms of the ethene part. Contour increments are 10^{-3} α-e au^{-3}.

methods compared to (localized) σ radicals; that is, these methods are less deficient when larger annihilation occurs at PUHF. Intuitively, one would reasonably have expected that the performance of the correlated methods would be best in the absence of spin contaminants in the reference function. Yet, just the opposite is true.

The hyperfine splitting constants a_H for allyl radical **A** are +4.06 for H1 and −14.83 and −13.93 for the CH_2 hydrogens H5 and H6, respectively. The signs of these a_H values agree well with the locations of α- and β-spin density in the spin density function of **A** (Figure 5). There also is qualitative but not quantitative agreement between these a_H values and the SP(H) data or the Fermi contacts (FC(H1) = +0.015; FC(H5) = −0.023; FC(H6) = −0.024) computed at the UHF level. The same is true for the QCISD and CISD data. However, such correlations should not be given much significance in light of our previous discussions[2] and because of the SP(H) data presented here. The substantial theoretical model dependencies discussed for the spin density functions in combination with the small magnitudes of the spin densities at the H atoms cause large variations in SP(H) depending on the method. At the PUHF level, for example, all the SP(H) values are positive and

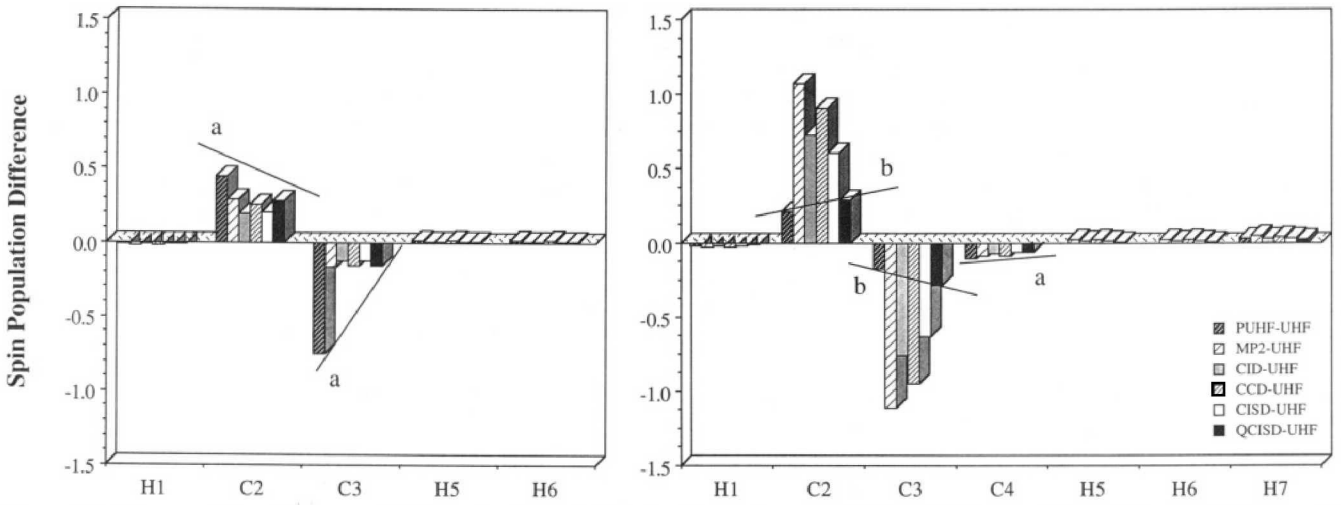

Figure 10. Spin population differences ΔSP^M for the theoretical levels (from left to right) PUHF, MP2, CID, CCD, CISD, and QCISD for all atoms of allyl radical in conformations **A** (left) and **B** (right). The conditions $|\Delta SP^{PUHF}| > |\Delta SP^{QCISD}|$ and $|\Delta SP^{PUHF}| < |\Delta SP^{QCISD}|$ are indicated by the lines marked "a" and "b", respectively.

SCHEME 1

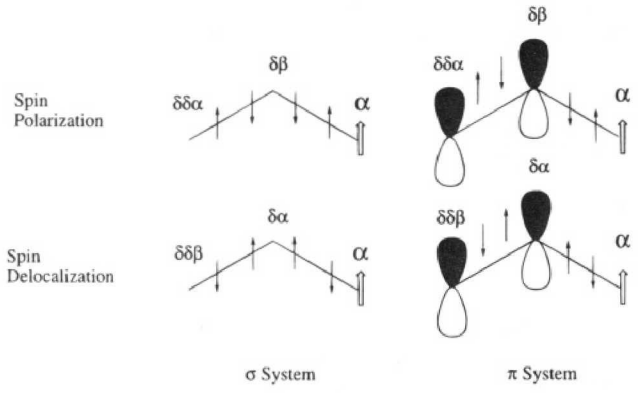

in a small range, $+0.004 < SP(H) < 0.005$, while they all are negative at the levels MP2 and CID.

Spin Delocalization versus Spin Polarization. Several important conclusions resulted from the analysis of the spin density functions. While the spin density functions for **A** are qualitatively affected in the same fashion at all of the correlated levels, the spin polarization patterns of **B** depend dramatically on the correlation method. For **B**, only the UHF and PUHF methods yield spin density functions that are in good agreement with the QCISD results; ϱ^S(QCISD), ϱ^S(UHF), and ϱ^S(PUHF) show the same spin polarization at all C atoms, and there are only differences at the in-plane methylene H atoms (which carry marginal spin density). All of the other methods (MP2, CID, CCD, and CISD) indicate erroneous spin polarizations in the $H_2C{=}CH-$ fragment of **B**. All of these findings can be consistently explained by theoretical model-dependent differences in the relative importance of "spin polarization" and "spin delocalization".

An unpaired α-spin electron may affect the remainder of the paired electrons either via spin polarization or via spin delocalization. These two possibilities are depicted in Scheme 1 for the σ and the π systems. The unpaired electron is symbolized by "$\Uparrow$", and the spins of paired electrons are shown as "↑" and "↓". We begin with the discussion considering the case where the unpaired electron is localized (on the atom to the right in Scheme 1), as is the case for **B**. The basic idea of spin polarization is that the electrons in bonds connected to the radical site are affected in such a way as to increase the probability of finding the bonding α-spin electron close to the site of the unpaired α-spin electron. This mechanism increases the α-spin even more at the site of the unpaired electron and leads to β-spin density at atoms that are one (or an odd number of) σ bond(s) removed from the radical center and to α-spin density at atoms that are two (or an even number of) σ bonds removed from the radical center. The magnitude of this effect should decline with distance (as indicated by $\delta\beta$ and $\delta\delta\alpha$). Spin delocalization, on the other hand, occurs when the interaction of the unpaired electron with the bonds is just the opposite as shown in the bottom row of Scheme 1. The spin density in the region of the radical site is reduced because the bond electrons are correlated in such a way as to place the bond β-spin orbital closer to the radical site. Spin delocalization leads to small α-spin density accumulations at atoms that are one (or an odd number of) σ bond(s) removed from the radical center and to smaller β-spin density accumulations at atoms that are two (or an even number of) σ bonds removed from the radical center. The mechanisms have the same result no matter whether we consider σ or π MOs as mediators of spin polarization or delocalization. To the right in Scheme 1, the possible spin propagations are shown when mediated by a σ,π bond sequence.

For **A**, these same mechanisms of spin polarization and spin delocalization have to be considered in the same way. The difference is only that the unpaired electron occupies a π MO which places α-spin density at the two terminal C atoms. The overall effects of spin polarization and spin delocalization mediated via the σ framework now emerge as the superposition of the effects of the unpaired α-spins at two sites. Since the sites of unpaired α-spin are two bonds removed, the effects of each on the central CH units are the same. The spin delocalization is enhanced in this case because the $\delta\delta\beta$ effect of one spin site reduces the α-spin even more at the other. The interaction of the unpaired α-spin electron with the two electrons of the bonding π MO must involve spin polarization and cause $\delta\beta$ at the central C atom for symmetry reasons.

For allyl radical **A**, our results demonstrate that spin polarization dominates spin delocalization. At all levels, we find spin density functions that show β-spin density at the central C atom. If spin delocalization in the σ framework were to dominate, we would find α-spin density at the central C atom. Moreover, we find that the relative importance of spin polarization is reduced once electron correlation effects are included, but it remains the dominant mode of interaction between the unpaired electron and the paired electrons. For **B**, the situation is complicated by the theoretical level dependencies described above. At the HF and at the QCISD levels, we find that spin

polarization is again the dominant mechanism for the interaction of the spin of the unpaired electron with the paired electrons. However, the spin density distributions within the ethene part of **B** determined at the MP2, CID, CCD, and CISD levels all would predict that spin delocalization was more important than spin polarization. We can therefore summarize our analyses of the electron and spin density functions of allyl radical with the statement: *The theoretical model dependencies described are due to the underestimation of the spin polarization interaction of the unpaired electron with the paired electrons in conformation **B** of allyl radical at the MP2, CID, CCD, and CISD levels.*

One may wonder how these changes in the *spin density* distribution are related to the *electron density* distribution. The results obtained for all correlated levels agree in predicting reductions in the electron density in the bonding regions and increases of electron density in the atomic regions. It is the very idea of electron correlation, of course, to allow electrons to get closer to the nuclei while reducing electron−electron repulsion via correlation of the motions of the α and β electrons. *All post-HF methods show the same trend in their effects on the electron density.* Moreover and not as obvious, *all post-HF methods also show the same trend in their effects on the spin density distribution in that electron correlation always increases the relative importance of the spin delocalization mechanism.* For QCISD, the relative importance of spin delocalization is increased but remains less than spin polarization. For the other correlated methods, the relative importance of spin delocalization also is increased, but, in these cases, it becomes dominant for the **B** structures but not for the **A** conformations.

The terms spin delocalization and electron delocalization should be carefully separated. The term spin delocalization refers to the interaction of an unpaired electron in one MO with the paired electrons in the other MOs, and *a priori* this interaction can occur whether the unpaired electron occupies a localized or a delocalized MO. Our analysis of allyl radical in conformations **A** and **B** shows that, at least in this case, the importance of spin delocalization is less for the (electron-) delocalized system **A** than for the (electron-) localized system **B**.

Conclusion

The rotational automerization of allyl radical $\mathbf{A} \rightarrow \mathbf{B}^{\ddagger} \rightarrow \mathbf{A}$ was examined in detail at the theoretical levels UHF, PUHF, MP2, CID, CCD, CISD, and QCISD. Characteristics of the automerization path and of the relevant stationary structures, vibrational analyses, and activation energies were compared and revealed the unexpected occurrence of methodological deficiencies at the MP2, CID, CCD, and CISD levels. The analysis of the theoretical model dependencies of the structures and of the vibrational data provided a first indication that these deficiencies are related to problems with the electronic structure of the ethene part in conformation **B** and not with the electronic structure of allyl radical **A**. The graphical analysis of electron and spin density functions and of electron and spin density difference functions of **A** and **B** and the discussion of integrated electron and spin populations led to the discovery of the underlying fundamental problem. All methods describe the *electron density relaxation* along the automerization path well with only minor qualitative differences. All post-HF methods also show *the same trend* in the way they affect the spin density distribution in that electron correlation always increases the relative importance of the interaction of the unpaired electron with the paired electrons via the spin delocalization mechanism. The methods differ greatly, however, in the magnitude of this effect relative to the spin polarization mechanism, and major differences in the description of the *spin density relaxation* along the automerization path are the consequence.

The structure of **A** and the activation barrier computed at the highest level agree excellently with available experimental data. In general, there are only small theoretical model dependencies on structures, while the activation barriers are more sensitive. All methods also agree in describing the electron density distributions and the electronic relaxation along the automerization path, while model dependencies on the spin density distributions are the most significant. The spin density function analysis and the spin populations for the CH_2 and CH fragments of **A** indicate spin polarization with spin populations in excess of 0.5 α-e at the CH_2 groups and β-spin density at the CH group. The same type of spin polarization occurs at all levels, and spin polarization is reduced compared to the UHF reference. For **B**, all methods predict total spin populations at the rotating CH_2 group that are *less than unity,* but they greatly differ with regard to the *spin polarization within the ethene part.* UHF indicates significant $-(\beta)HC{=}CH_2(\alpha)$ spin polarization; spin projection reduces and QCISD theory nearly eliminates this spin polarization. All other methods would indicate spin polarizations within the ethene fragment that are *much larger than at the UHF level* and *of opposite polarity*: $-(\alpha)HC{-}CH_2{-}(\beta)$. The theoretical model dependencies are due to the underestimation of the spin polarization interaction of the unpaired electron with the paired electrons in conformation **B** of allyl radical at the MP2, CID, CCD, and CISD levels. For QCISD, the relative importance of spin delocalization is increased but remains less than spin polarization. For the other correlated methods, the relative importance of spin delocalization also is increased (in the order CISD, CCD, CID, and MP2), but, in these cases, it becomes dominant for the **B** structures but not for the **A** conformations. Our analyses of allyl radical show that the importance of spin delocalization is less for the delocalized radical **A** than for the localized radical **B**. It is also found that the MP2, CID, CCD, and CISD methods are less deficient when larger annihilation occurs at PUHF; that is, the deficiencies of these correlated methods are not the consequence of the presence of spin contaminants in the reference function. Future studies will have to establish whether these findings are of a more general nature.

Our results show that theoretical studies of open-shell systems with the MP2, CID, CCD, and CISD methods may suffer from serious deficiencies as the result of inadequate descriptions of the spin density distributions. The QCISD method yields results that are in very good agreement with all available experimental data. Our previous studies as well as the results presented here show the PUHF method to be a valuable alternative for studies of spin density distributions in general and in particular for large molecules, that is, for radicals where QCISD calculations are too computationally intensive.

Acknowledgment is made to the donors of the Petroleum Research Fund, administered by the American Chemical Society, for support of this work (PRF 24399-G4 and PRF 27139-AC4). We gratefully thank the MU PRIME FUND matching funds for the purchase of a computer system. We thank the reviewer for bringing ref 31 to our attention.

References and Notes

(1) (a) Part of the Ph.D. dissertation of G. S.-C. Choy. (b) Part 2 in the series Topological Electron and Spin Density Analysis of Radicals; for parts 1 and 3 see ref 2. (c) Presented at the XXVII Midwest Theoretical Chemistry Conference, Columbia, Missouri, May 1994, and at the 208th National ACS Meeting, Washington, DC, August 1994.

(2) (a) Glaser, R.; Choy, G. S.-C. *J. Phys. Chem.* **1993**, *97*, 3188. (b) Choy, G. S.-C.; Glaser, R. Submitted.

(3) (a) Wilk, R. D.; Cernansky, N. P.; Pitz, W. J.; Westbrook, C. K. *Combust. Flame* **1989**, *77*, 145. (b) Weissman, M.; Benson, S. W. *Prog. Energy Combust. Sci.* **1989**, *15*, 273. (c) Morgan, C. A.; Pilling, M. J.; Tulloch, J. M.; Ruiz, R. P.; Bayes, K. D. *J. Chem. Soc., Faraday Trans. 2* **1982**, *78*, 1323. (d) Tulloch, J. M.; Macpherson, M. T.; Morgan, C. A.; Pilling, M. J. *J. Phys. Chem.* **1982**, *86*, 3812. (e) Bergh, H. E. van den; Callear A. B. *Trans. Faraday Soc.* **1970**, *66*, 2681. (f) Lodhi, Z. H.; Walker, R. W. *J. Chem. Soc., Faraday Trans.* **1991**, *87*, 681. (g) Hanning-Lee, M. A.; Pilling M. J. *Int. J. Chem. Kinet.* **1992**, *24*, 271.

(4) Tiesler, A.; Zott, H.; Heusinger, H. *Radiat. Phys. Chem.* **1981**, *17*, 141.

(5) Carter, R. N.; Anton, A. B.; Apai, G. *J. Am. Chem. Soc.* **1992**, *114*, 4410.

(6) Vajda, E.; Tremmel, J.; Rozsondai, B.; Hargittai, I.; Maltsev, A. K.; Kagramanov, N. D.; Nefedov, O. M. *J. Am. Chem. Soc.* **1986**, *108*, 4352.

(7) (a) Fessenden, R. W.; Schuler, R. H. *J. Chem. Phys.* **1963**, *39*, 2147. (b) Kochi, J. K.; Krusic, P. J. *J. Am. Chem. Soc.* **1968**, *90*, 7157.

(8) Houle, F. A.; Beauchamp, J. L. *J. Am. Chem. Soc.* **1978**, *100*, 3290.

(9) (a) Meltsev, A. K.; Korolev, V. A.; Nefedov, O. M. *Izv. Akad. Nauk. SSSR, Ser. Khim.* **1982**, 2415. (b) Meltsev, A. K.; Korolev, V. A.; Nefedov, O. M. *Izv. Akad. Nauk. SSSR, Ser. Khim.* **1984**, 555. (c) Maier, G.; Reisenauer, H. P.; Rohode, B.; Dehnicke, K. *Chem. Ber.* **1983**, *116*, 732. (d) Huang, J. W.; Graham, W. R. M. *J. Chem. Phys.* **1990**, *93*, 1583. (e) Holthauer, K.; Cometta-Morini, C.; Oth, J. F. M. *J. Phys. Org. Chem.* **1990**, *3*, 219.

(10) (a) Getty, J. D.; Kelly, P. B. *Chem. Phys.* **1992**, *168*, 357. (b) Liu, X.; Getty, J. D.; Kelly, P. B. *J. Chem. Phys.* **1993**, *99*, 1522. (c) Getty, J. D.; Burmeister, M. J.; Westre, S. G.; Liu, X.; Kelly, P. B. *J. Am. Chem. Soc.* **1991**, *113*, 801. (d) Getty, J. D.; Liu, X.; Kelly, P. B. *Chem. Phys. Lett.* **1993**, *201*, 236.

(11) McKelvey, J.; Hehre W. *J. Mol. Phys.* **1973**, *25*, 983.

(12) McKelvey, J.; Berthier, G. *Chem. Phys. Lett.* **1976**, *41*, 476.

(13) Paldus, J.; Veillard, A. *Chem. Phys. Lett.* **1977**, *50*, 6.

(14) Kikuchi, O. *Chem. Phys. Lett.* **1980**, *72*, 487.

(15) Szalay, P. G.; Császár, A. G.; Fogarasi, G.; Karpfen, A.; Lischka, H. *J. Chem. Phys.* **1990**, *93*, 1246.

(16) (a) Schleyer, P. v. R. *J. Am. Chem. Soc.* **1985**, *107*, 4793. (b) Olivella, S.; Solé, A.; Bofill, J. M. *J. Am. Chem. Soc.* **1990**, *112*, 2160. (c) Cometta-Morini, C.; Ha, T.-K.; Oth, J. F. M. *J. Mol. Struct.* (THEOCHEM) **1989**, *188*, 79. (d) Fjogstad, E.; Ystenes, M. *Spectrochim. Acta* **1990**, *46A*, 47. (e) Hammons, J. H.; Coolidge, M. B.; Borden, W. T. *J. Phys. Chem.* **1990**, *94*, 5468. (f) Coolidge, M. B.; Hrovat, D. A.; Borden, W. T. *J. Am. Chem. Soc.* **1992**, *114*, 2354. (g) Nicolaides, A.; Borden, W. T. *J. Am. Chem. Soc.* **1992**, *114*, 8682.

(17) Levin, G.; Goddard, W. A., III. *J. Am. Chem. Soc.* **1975**, *97*, 1649.

(18) (a) The terms "allyl resonance energy" and "allyl stabilization energy" differentiate between these two methods: Doering, W. v. E.; Roth, W. R.; Breuckmann, R.; Figge, L.; Lennartz, H.-W.; Fessner, W.-D.; Prinzbach, H. *Chem. Ber.* **1988**, *121*, 1. (b) Korth, H.-G.; Trill, H.; Sustmann, R. *J. Am. Chem. Soc.* **1981**, *103*, 4483. (c) Golden, D. M.; Benson, S. *Chem. Rev.* **1969**, *69*, 125.

(19) Krusic, P. J.; Meakin, P.; Smart, B. E. *J. Am. Chem. Soc.* **1974**, *96*, 6211.

(20) Hammons, J. H.; Coolidge, M. B.; Borden, W. T. *J. Phys. Chem.* **1990**, *94*, 5468.

(21) Feller, D.; Davidson, E. R.; Borden, W. T. *J. Am. Chem. Soc.* **1984**, *106*, 2513.

(22) Frisch, M. J.; Trucks, G. W.; Head-Gordon, M.; Gill, P. M. W.; Wong, M. W.; Foresman, J. B.; Johnson, B. G.; Schlegel, H. B.; Robb, M. A.; Replogle, E. S.; Gomperts, R.; Andres, J. L.; Raghavachari, K.; Binkley, J. S.; Gonzales, C.; Martin, R. L.; Fox, D. J.; Defrees, D. J.; Baker, J.; Stewart, J. J. P.; Pople, J. A. *Gaussian 92* (Rev. A); Gaussian Inc.: Pittsburgh, PA, 1992.

(23) (a) Hehre, W. J.; Ditchfield, R.; Pople, J. A. *J. Chem. Phys.* **1972**, *56*, 2257. (b) Hariharan, P. C.; Pople, J. A. *Theoret. Chim. Acta* **1973**, *28*, 213. (c) Binkley, J. S.; Gordon, M. S.; DeFrees, D. J.; Pople, J. A. *J. Chem. Phys.* **1982**, *77*, 3654.

(24) (a) Handy, N. C.; Schaefer, H. F., III. *J. Chem. Phys.* **1984**, *81*, 5031. (b) See ref 22.

(25) Choy, G. S.-C. Ph.D. Dissertation, University of Missouri, Columbia, MO, 1994.

(26) Glaser, R. Department of Chemistry, University of Missouri, Columbia, MO, 1990.

(27) (a) Löwdin, P. O. *Quantum Theory of Atoms, Molecules, and the Solid State;* Academic Press: New York, 1966; p 601. (b) For a recent discussion of spin contamination of UHF functions and their geometrical interpretation using Araki angle operators, see: Cassam-Chenai, P.; Chandler, G. S. *Int. J. Quantum Chem.* **1993**, *46*, 593.

(28) Löwdin, P. O. *Phys. Rev.* **1955**, *97*, 1509.

(29) See also: Marshall, W. *Proc. Phys. Soc., London* **1961**, *78*, 113.

(30) (a) Krishnan, R.; Binkley, J. S.; Seeger, R.; Pople, J. A. *J. Chem. Phys.* **1980**, *72*, 650. (b) McLean, A. D.; Chandler, G. S. *J. Chem. Phys.* **1980**, *72*, 5639.

(31) A precedent for this case has recently been described: Pauzat, F.; Ellinger, Y.; Berthier, G.; Gérin, M.; Viala, Y. *Chem. Phys.* **1993**, *174*, 71. UHF theory erroneously predicts an activation barrier for the reaction N + OH → NOH, which can be demonstrated to originate in a strong spin contamination by a low-lying quintet state.

(32) (a) Langhoff, S. R.; Davidson, E. R. *Int. J. Quantum Chem. Symp.* **1976**, *10*, 1. (b) Pople, J. A.; Seeger, R.; Krishnan, R. *Int. J. Quantum Chem. Symp.* **1977**, *11*, 149.

(33) Vajda, E.; Tremmel, J.; Rozsondai, B.; Hargittai, I.; Maltsev, A. K.; Kagramanov, N. D.; Nefedov, O. M. *J. Am. Chem. Soc.* **1986**, *108*, 4352.

(34) Szalay, P. G.; Császár, A. G.; Fogarasi, G.; Karpfen, A.; Lischka, H. *J. Chem. Phys.* **1990**, *93*, 1246.

(35) Hirota, E.; Yamada, C.; Okunishi, M. *J. Chem. Phys.* **1992**, *97*, 2963.

(36) (a) Takada, T.; Dupuis, M. *J. Am. Chem. Soc.* **1983**, *105*, 1583. (b) Reference 16b. (c) Reference 34. (d) Reference 16c. (e) Sim, F.; Salahub, D. R.; Chin, S.; Dupuis, M. *J. Chem. Phys.* **1991**, *95*, 4317.

(37) Vibrate—A Normal Mode Visualization Program. Version 2. Glaser, R.; Chladny, B. S.; Hall, M. K. *Quantum Chemistry Program Exchange, QCPE Bulletin* **1993**, *13*, 75.

(38) Numerical accuracy of the integrations are within 0.005.